The effect of surrounding air on tyre vibrations

The effect of surrounding air on tyre vibrations

J.P.M. Vissers

DCT 2004.58

TU/e technische universiteit eindhoven

Department of Mechanical Engineering

CHALMERS

Department of Applied Acoustics

J.P.M. Vissers s471788

Abstract

The goals of this research are to study to what extend the air in the narrow geometry between tyre and road will influence the vibrations and sound radiation of the tyre. To achieve these goals two different models are made using the "low reduced frequency model" described by Beltman. The first model consists of a patch vibrating just above the ground and the second model consists of a patch vibrating inside a tube. Both models are used in combination with input data from measurements and calculations to study the effect for different mechanisms that play a role in tyre/road noise. The main conclusions are that the air in the narrow geometry has an effect on the vibration of the tyre and that the radiated sound is not *directly* affected by the narrow geometry, but indirectly by the change of the vibration of the patch due to the narrow geometry.

Acknowledgements

I want to thank the whole Department of Applied Acoustics in Sweden for the great support and the nice environment. I especially want to thank Patrik Andersson for his supervision.
I also want to thank my home university in Eindhoven, the Chalmers University, professor H. Nijmeijer and professor W. Kropp to make it possible to have my 14-weeks traineeship in Sweden.

Chapter 1: Introduction

1.1: General Introduction

Noise, which is unwanted sound, has become an environmental pollution that affects most people's health, comfort or general well being during the last decades.
For example, it was concluded by Stanners & Bourdeau (1995 [13]) that approximately 20% of the population in the European Union is exposed to noise levels that are considered to be intolerable and 60% to levels which are considered as undesirable. Not even the remaining 40% would be enjoying a good acoustical environment, since the exposure levels would then need to be below approximately 45 dB(A).
Road traffic noise is traditionally associated with engine and exhaust noise of vehicles, but during the later part of the 20th century the emission and propagation of noise from these sources is partly reduced, while at the same time the noise emission from the tyre/road interaction on a relative scale becomes more and more prominent. Now it appears that tyre/road noise is the component that needs to be reduced more than anything else! This tyre/road noise is the main source of the noise if a car drives faster than 50 km/h and if a truck drives faster than 80 km/h [3].
There are two main mechanisms involved in tyre/road noise.
The *first* one is the vibration mechanism, where the vibration can be introduced by different mechanisms (stick/snap, tyre tread impact, road roughness etc).
The *second* mechanism is related to aerodynamics, i.e. the air that flows around the tyre will cause noise. Examples of this mechanism are air turbulence and air-pumping. All the mechanisms will be discussed in greater detail in Chapter 2.
In the last decade improvement in modeling and understanding of the problem is achieved for instance at the university of Chalmers. The model developed there is at this moment (2004) already quite accurate in predicting the radiated sound for tyres on normal road surfaces, but on smooth surfaces (i.e. highways in Germany and France) there is still a significant deviation between the results from the measurements and the model especially for high frequencies. A part of the reason of this difference is that adhesion and stick-slip are not modeled yet.
Further, what is not modeled yet is the effect of the surrounding air around the tyre on the tyre and most important the air in small gaps/layers between the tyre and the road. How much the tread blocks and the vibrating walls inside tyre grooves are affected by this air is still unknown. In this report two models will be developed that can simulate these two situations.
Knowing this all, the subject of this research can be defined as: vibrations in "narrow" geometries.
First the project objectives will be given and there will be a brief discussion of the mechanisms that are related to tyre/road noise. After this a brief description of the model developed at the Chalmers University will be given. Next the report will go on with a solution for two models that will be used to draw conclusions. The first model will be of a block vibrating just above the ground and the second will be a patch vibrating in a tube. Finally conclusions and recommendations will be given.

1.2: Project objectives

The *objectives* of this project are:
* To investigate to what extent the dynamic load of the surrounding air will influence the vibrations on a tyre during tyre/road interaction.
* To investigate to what extent the narrow geometry will influence the radiation from the contact patch.

To be able to say something about the objectives two different models will be used.
Model A is a vibrating object in front of a rigid surface and model B is a patch vibrating in a tube.
These two models are both "simple" models that can be used to study some general parameters such as amplitude, distance between object and surface, forces, noise radiation etc.

Chapter 2: Overview of Tyre/road noise

An overview of the tyre/road noise in combination with the related generation mechanisms and the Chalmers model will be given as an introduction into the back ground of this report.

2.1: Tyre/road noise introduction

2.1.1: Tyre/road noise as part of vehicle noise

Vehicle noise can be divided in 3 parts; wind turbulence noise (chassis), power unit noise (i.e. engine, gearbox and differential) and tyre/road noise. From the general frequency characteristic of the total noise of a vehicle (figure 2.1 [3]) it can be concluded that there is a peak around 1000 Hz.

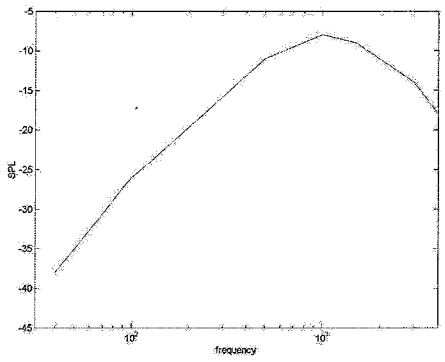

Figure 2.1: The peak around 1000Hz (Normalized to –8 dB) [3]

Above a certain driving speed the tyre noise starts to dominate over power unit noise. This "crossover" speed is for each car different, but for a normal car it is around the 50 km/h.[3].

2.1.2: Wave types along the circumference of the tyre

The waves in the circumference of the tyre will be discussed, because these are important for the understanding of the total problem and for the assumptions made in the model(s).
The vibrations of the belt consist of three types of waves ([3] and [4]).
Type1: This type mainly represents the radial motion of the belt. At low frequencies it corresponds to membrane waves (loss factor 0.05-0.1), which at higher frequencies (250 Hz) are changed into bending waves (loss factor 0.2-0.45), which are a better "radiator" because of the higher loss factor.
Type 2: This type corresponds to longitudinal waves similar to waves on a beam. This type has a cut off frequency given by the ring frequency, which is 400 Hz for usual passenger car tyres).
Type 3: This is a shear wave where the outer surface of the soft rubber tread layer and the stiff steel reinforced belt are vibrating out of phase relative to each other.

2.2: Tyre/road noise sources and generation mechanisms

In the next part the tyre/road noise generation mechanisms and the amplification or reduction mechanisms will be discussed. It is important to mention what type of

mechanisms there are, because they are the inputs for the systems that are going to be studied here.

2.2.1: Tyre/road noise generation mechanisms

Tyre/road noise generation mechanisms can be divided into 2 main groups [3]:

1) Vibrational (structure-borne)

Impact mechanisms

Tyre tread impact: Impact of the tyre tread blocks which cause radial and tangential vibrations in the tyre tread and belt, spreading to the sidewalls.

Road texture impact: Impact of road surface texture on the tyre tread, which have the same effect as the impact of the tyre tread blocks.

Running deflection: Deflection of tyre tread at leading and trailing edges due to the non-circular shape of a mounted tyre, giving the belt/carcass vibrations.

Adhesion mechanisms

Stick/slip tread element motions relative to the road surface, causing tangential tyre vibrations, also called "scrubbing"

Rubber to road *stick/snap* (adhesive effect); giving either tangential or radial vibrations

2) Aerodynamical (air-borne)

Air displacement mechanisms

Air turbulence: Turbulence around a tyre due to the tyre displacing air when rolling on the road and air dragged around by the spinning tyre/rim.

"Air-pumping": Air displaced into/out of cavities in or between tyre tread and road surface, without necessarily being in resonance

Pipe resonances: Air displacement in grooves ("pipes") in the tyre tread pattern amplified by resonances, so-called $\lambda/2$ and $\lambda/4$ resonators

Helmholtz resonance: Air displacement into/out of connected air cavities in the tyre tread pattern and the road surface amplified by resonances

Research of noise-texture and vibration-noise relations has been performed by Sandberg & Descornet [3]. A result from this research is that at low frequencies the vibration mechanism is most important and that at high frequencies the aerodynamical mechanism is most important.

Almost all the mechanisms play a role in this report, but the most important mechanisms for this report are stick/slip, air-pumping, running deflection and stick/snap. These can be seen as a direct input for the parameters of the models.

2.2.2: Amplification or reduction mechanisms

Here a summary of the amplification and reduction mechanisms that play a role in tyre/road noise is given. A more detailed description of each part can be found in [3].

- *Torus cavity resonance in the tyre tube*
  Resonance of the medium inside the tyre.
- *Horn effect*
  The amplification because of the "horn" formed by the tyre and the road.
- *Mechanical impedance influence*
  The influence of the stiffness/impedance of the road to tyre noise.
- *Sound radiation from the road*
- *Acoustical impedance effect*
  How voids in the road influence the absorbing of the noise.
- *Tyre resonance*

2.3: Tyre/Road noise modeling

There are several institutes that develop models that model tyre/road noise. In general there is still some discussion about the modeling of the air pumping mechanism, because it is not clear how to model it properly. For instance M.J.Gagen (1999) [9] concludes that the monopole theory and the $\lambda/4$ theory, which are both used for squeezed cavity, are not a complete explanation for the noise. He concludes that the squeezed acoustic wave equation is maybe a better way to model the squeezed cavity. He shows that the usual assumption of a small amplitude acoustic wave equation and the acoustic monopole theory derived from this equation is incorrect for squeezed systems, because the amplitude of the pressure and density are so large that the small amplitude acoustic monopole theory and the $\lambda/4$ theory are not good approaches anymore. There is however still a huge discussion about these conclusions. This report is more focused on the effect of the vibration of walls than the effects due to the compression of the cavity. However later on some effects studied by Gagen [9] (i.e. the increased density) maybe can be taken into account to improve the model for the tubes/grooves of the tyre.
In the Chalmers model (Krister Larsson [8]) the air pumping is modeled using the tread deformation as an input. The volume change between road and tyre caused by the local deformation of the tread is used as an input to calculate (some of) the air pumping. Hence, the air pumping mechanism is sometimes termed as local deformation by Chalmers.

2.3.1: The Chalmers model

The Chalmers model is one of the so-called "complete" models, which means that it tries to simulate the total tyre/road noise problem. It consists of 3 main parts: the tyre model, the contact model and the radiation model.
The *tyre model* is a flat double-layered plate supported by springs where the top layer represents the tread cap and the second layer represents the rim. The springs represent the support by the sidewalls and the air load. Each layer is modeled as an elastic solid, governed by elastic field equations.
The *contact model* consists of a set of Green's functions pre-calculated with the tyre model, which define the relation between the contact force and the deformation. In the latest contact model the coupling between all contact points are taken into account using an elastic halfspace.
The *radiation model* consists of 2 multipoles, which reduce the problem to a 2D radiation-model. The Horn effect and the reflection properties of the road are taken into account.

In this report the focus will be on the problem that at this moment the model is in some kind of "vacuum". The effect of the surrounding air on the vibrations of the tyre is not modeled. To find if there is an effect two models will be discussed and later on conclusions about the size of the effect will be made using those two models.

Chapter 3: Literature study of air behavior in small gaps

The literature is found in 3 different ways: handed out by the coach at the department, the Internet and library in the department. Several papers are found but the papers of Gagen and Beltman appeared to be very useful. The paper of Gagen [3] is about the modeling of the squeezing of a tyre cavity using the squeezed acoustic wave equation. The paper of Beltman focuses more on a patch vibrating above a plate and more of those examples. From this paper the low reduced frequency model will be discussed, because this model will be used to develop the models that can be used to say something about the objectives of this report.

3.1: The low reduced frequency model

In the paper by Beltman [1] a model is introduced which is called *the low reduced frequency model.* It is a model with dimensionless parameters that is derived from the linearized Navier Stokes equations, the equation of continuity, the equation of state for an ideal gas and the energy equation. Some assumptions are made from which the most important ones are: small sinusoidal perturbations, the acoustic wavelength is large compared to the length scale (l) and the acoustic wavelength is large compared to the boundary layer thickness. The length scale can for instance be seen as the distance between a patch and the ground. The solution strategy is based on the fact that the pressure is constant over the cross section. This means that the temperature perturbation can be solved from a Poisson type of equation after which the velocity and density profile can be calculated in the same way. These three equations can now be inserted in the equation of continuity and after integration with respect to the cross-sectional coordinate(s) the basic formula of the low reduced frequency is found.

First the basic equations are formulated, cf. [1].

$$\rho_0 \frac{\partial \overline{v}}{\partial t} = -\overline{\nabla}\overline{p} + (\frac{4}{3}\mu + \eta)\overline{\nabla}(\overline{\nabla}\cdot\overline{v}) - \mu\overline{\nabla}\times(\overline{\nabla}\times\overline{v}) : \text{The linearized NS eq.} \quad (1)$$

$$\rho_0(\overline{\nabla}\cdot\overline{v}) + \frac{\partial\overline{\rho}}{\partial t} = 0 : \text{The equation of continuity.} \quad (2)$$

$$\overline{p} = \overline{\rho}R_0\overline{T} : \text{The equation of state for an ideal gas.} \quad (3)$$

$$\rho_0 C_p \frac{\partial \overline{T}}{\partial t} = \lambda\overline{\Delta}\overline{T} + \frac{\partial\overline{p}}{\partial t} : \text{The energy equation.} \quad (4)$$

where $\overline{v}$ is the velocity vector, $\overline{p}$ is the pressure vector, $\overline{T}$ is the temperature, $\overline{\rho}$ is the density, ρ_o is the mean density, η is the viscosity, μ is the bulk viscosity, R_0 is the gas constant, λ is the thermal conductivity, C_p is the specific heat at constant pressure, t is the time, $\overline{\nabla}$ is the gradient operator and $\overline{\Delta}$ is the Laplace operator.

To get to these equations the following assumptions are made:
There is no internal heat generation, there is a homogeneous medium, there is no mean flow, there is a laminar flow and there are small sinusoidal perturbations that can be formulated as:

$$\overline{v} = c_0 v e^{i\omega t} \quad (5)$$

$$\overline{T} = T_0(1 + Te^{i\omega t}) \quad (6)$$

$$\overline{p} = p_0(1 + pe^{i\omega t}) \quad (7)$$

$$\overline{p} = \rho_0 (1 + \rho e^{i\omega t}) \tag{8}$$

where v is the dimensionless velocity, c_0 is the undisturbed speed of sound, T_0 is the mean temperature, T is the dimensionless temperature, p_0 is the mean pressure, p is the dimensionless pressure, ρ is the dimensionless density.

The model is a model with dimensionless parameters from which the shear wave number (s) and the reduced frequency (k) are the most important ones. These are defined as:

$$s = l\sqrt{\frac{\rho_0 \omega}{\mu}} \tag{9}$$

$$k = \frac{\omega l}{c_o} \tag{10}$$

where l is the length scale and ω is the angular frequency.

The low reduced frequency model is derived from the (dimensionless) basic equations under the additional assumptions: k<<1, which means that the acoustic wavelength is large compared to the length scale l and k/s<<1, which means that the acoustic wavelength is large compared to the boundary layer thickness.
With these additional assumptions the basic equations result in [1]:

$$iv^{pd} = -\frac{1}{k\gamma}\nabla^{pd} p + \frac{1}{s^2}\Delta^{cd} v^{pd} \tag{11}$$

$$0 = -\frac{1}{k\gamma}\nabla^{cd} p \tag{12}$$

$$\nabla \cdot v + ik\rho = 0 \tag{13}$$

$$p = \rho + T \tag{14}$$

$$iT = \frac{1}{s^2\sigma^2}\Delta^{cd} T + i\left[\frac{\gamma - 1}{\gamma}\right]p \tag{15}$$

where v^{pd} is the velocity in the propagation coordinate(s) direction, γ is the ratio of specific heats, ∇^{pd} is the gradient operator in the propagation coordinates, Δ^{cd} is the Laplace gradient in the cross-sectional coordinates and σ is the square root of the Prandtl number.

The solution strategy is based on three steps:

1) The pressure is a function of the propagation coordinates only so the pressure is constant on a cross section or across the layer thickness. This is also the reason why low reduced frequency models are sometimes referred to as constant pressure models.
2) Using the fact that the pressure does not vary in the thickness direction of the layer the temperature perturbation can be solved from a Poisson type of equation.
3) After the solution from the temperature profile is obtained, the velocity and density profile can be obtained as well.

The expressions for density, temperature and velocity are now inserted into the equation of continuity. Before quoting the formulas the boundary conditions needed to solve the problem can be defined:

- The continuity of velocity: The tangential velocity at the walls is zero, so a no-slip condition is imposed. The normal velocity is equal to the velocity of the wall(s) [1].
- The temperature boundary conditions are isothermal walls or adiabatic walls in common boundary conditions. For an isothermal wall the temperature perturbation is zero, but for an adiabatic wall the gradient of the temperature normal to the wall vanishes [1].
- The pressure at the end of a tube or layer can be defined (for instance zero or with an end-impedance).

Now the resulting basic equations after integration with respect to the cd-coordinate are:

$$\Delta^{pd} p(x^{pd}) - k^2\Gamma^2 p(x^{pd}) = -ikn(s\sigma)\Gamma^2\Re \tag{16}$$

$$\Gamma = \sqrt{\frac{\gamma}{n(s\sigma)B(s)}} \tag{17}$$

$$n(s\sigma) = \left[1 + \left[\frac{\gamma - 1}{\gamma}\right] D(s\sigma)\right]^{-1} \tag{18}$$

$$B(s) = \frac{1}{A^{cd}} \int_{A^{cd}} A(s, x^{cd}) dA^{cd} \tag{19}$$

$$D(s\sigma) = \frac{1}{A^{cd}} \int_{A^{cd}} C(s\sigma, x^{cd}) dA^{cd} \tag{20}$$

$$\Re = \frac{1}{A^{cd}} \int_{\delta A^{cd}} v \bullet e_n d\partial A^{cd} \tag{21}$$

where x^{cd} are the coordinate(s) of the cross section, x^{pd} are the coordinate(s) in the propagation direction, A^{cd} the cross-sectional area, $\Re$ is the function which states how and which part of "the construction" vibrates, A is the function describing velocity and temperature profiles, C is the function describing the temperature profile, $n(s\sigma)$ is the polytropic constant, B is the function accounting for viscous or thermal effects, Γ is the propagation constant and D is the function describing the temperature profile.

In general the absolute value of $n(s\sigma)$ goes to 1.4 for high values of $(s\sigma)$ (>10) and for low values of $(s\sigma)$ (<1) the absolute value goes to 1. The absolute value of A has a parabolic profile for low shear wave numbers (viscous forces dominate) and for high shear wave numbers it has a flat velocity profile (inertial forces dominate).
For isothermal walls A and C are directly related, $C(s\sigma,x^{cd})=A(s\sigma,x^{cd})$ and for adiabatic walls $C(s\sigma,x^{cd})= -1$. For isothermal walls D and B are directly related, $D(s\sigma)=B(s\sigma)$ and for adiabatic walls $D(s\sigma)= -1$.
By Beltman [1] it is concluded that the low reduced frequency models can be used in most viscothermal problems under normal circumstances (atmospheric conditions and normal temperatures). The full linearized Navier Stokes model is only needed under extreme conditions, because for "normal" conditions there are more simple models available that also give accurate results.

Chapter 4: Model A: a vibrating object in front of a rigid surface

In this chapter model A: a vibrating object in front of a rigid surface will be discussed. This model is developed to simulate the forces on the tyre treads at the trailing and leading edge during driving. The tyre treads are vibrating just above the ground due to the mechanisms discussed in chapter 2. The dimensions of the object of the model will be the same as the dimensions of an ordinary tyre tread blocks. At the end of this chapter some general conclusions about the model will be made.

4.1: Model

The model layout is shown in figure 4.1. Here the mean distance between the plate and the fixed surface is defined as $2h_0$. The amplitude will be defined as $h_0 h$ so the distance between the plate and the fixed surface is defined as:

$$h(t)=h_0(2+he^{iwt}) \tag{22}$$

Where h is the dimensionless amplitude.

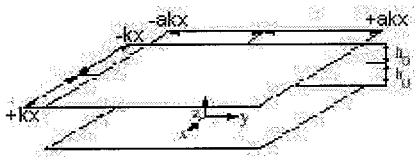

Figure 4.1: Layout of problem 1 (see also appendix B and [1])

where k_x is defined as:

$$k_x = \frac{\omega l_x}{c_0} \tag{23}$$

As stated in chapter 3 boundary conditions for the pressures at the edges are needed to solve the problem. Because it is a model with dimensionless parameters the boundary conditions are introduced at x=+/- k_X and y=+/- ak_X where k_x is the wave number and a is l_y/l_x, where l_y and l_x are the half-lengths of the plate (dimensions: $2l_x$ x $2l_y$) (see also appendix B). At the boundaries, which are here the ends of the plate, it is assumed that the pressure is zero. This is a simplification, since the pressure distribution outside the gap will be affected by the pressure distribution in the gap and vice versa. For narrow gaps the magnitude of the pressure perturbation in the gap is very large compared to the magnitude of the pressure perturbation outside the gap, so the boundary condition p=0 is a good approximation, which is confirmed by Beltman [1].

This all results in the formula for a rectangular plate (see appendix B for the derivation):

$$\frac{\partial^2 p}{\partial x^2}+\frac{\partial^2 p}{\partial y^2}-\Gamma^2 p = n(s\sigma)\Gamma^2 \frac{1}{2}h \tag{24}$$

$$B(s)=\frac{\tanh(s\sqrt{i})}{s\sqrt{i}}-1 \tag{25}$$

$$n(s\sigma)=\left[1+\left[\frac{\gamma-1}{\gamma}\right]D(s\sigma)\right]^{-1} \tag{26}$$

Formulas for the pressure, the force on the plate and the transfer function are formulated from these equations using the boundary conditions. The results from these formulas are dimensionless pressures and forces. To get the real pressures the

dimensionless pressures must be multiplied by p_o (mean temperature outside). To get the real forces on the patch the dimensionless force must be multiplied by $l_x l_y p_o$ [1].
Beltman has done experiments to validate the model from which the results produced (experiments and model) are shown in [1]. He concludes that the low-reduced frequency model gives a good description of the shift of the eigenfrequencies and pressures of the problem.

4.2: Validation m-file/model

The formulas from the literature are implemented in Matlab and are validated by reproducing the results shown in [1] at page 74, 75 and 76. The validation can be seen in appendix A.
Rhe conclusion from the validation can be that the isothermal wall approach gives a better estimation of the pressures and the eigenfrequencies of the experiments. It looks like the model *under* predicts the pressures for small gaps if the adiabatic, inviscid system is used and *over* predicts the eigenfrequency. That is the reason why in this report the approach of the *isothermal, viscid system* will be used.

4.3: The usefulness of the low frequency model for the tyre/road noise problem

To be sure that the low reduced frequency model is useful to study tyre treads vibrating just above the ground two things are checked:

1) First there are 2 restrictions to 2 dimensionless numbers;
   $k << 1$ and $k/s << 1$
2) Second there is a boundary condition for the pressure at the edges ($p=0$), which is a good approximation only if the pressure distribution outside the gap is very small compared to the pressure in the gap.

To study these limitations some typical values of tyre treads are chosen. Because the model is suitable for a patch vibrating above the ground there is chosen to model tyre tread blocks instead of the whole tread. In general the length and width of a tyre tread block are about 20 mm x 20 mm maximum.
The frequency range of interest is between 0 and 4000 Hz, because in this region all the main effects of tyre/road noise appear and also the eigenfrequency of interest of a "normal" tyre tread block is in this region [8].

4.3.1: The dimensionless factors k and k/s

k And k/s are checked for the frequency range of 0-4000 Hz.
What can be concluded is that k/s is always much smaller than 1. The problem is the condition $k<<1$, because this becomes critical (>0.2) for higher frequencies if the gap is larger than 5mm. It is assumed that the model still gives an indication for gaps from 5 mm - 10 mm. For larger gaps the model will get less and less valid, but gaps larger than 10 mm are not interesting for the effects studied in this report.

4.3.2: pressure distribution

To check the boundary condition $p=0$ a plot is made for four different gap heights. In figure 4.2 the line of the maximum real pressure ($p_0 * p$) divided by the real amplitude ($h_0 h$) is plotted, so for instance if the gap is 0.1 mm and the amplitude is 0.01mm then the real maximum pressure would be the pressure in figure 4.2 multiplied by 0.01.

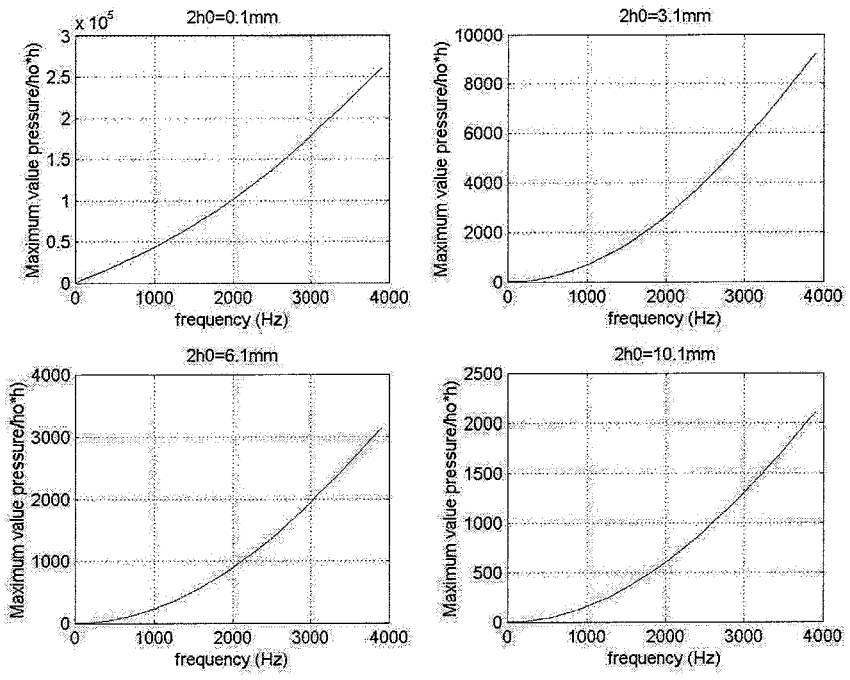

Figure 4.2: Maximum pressure/amplitude for different widths of the gap

Examples of the pressure distribution on the tyre tread:

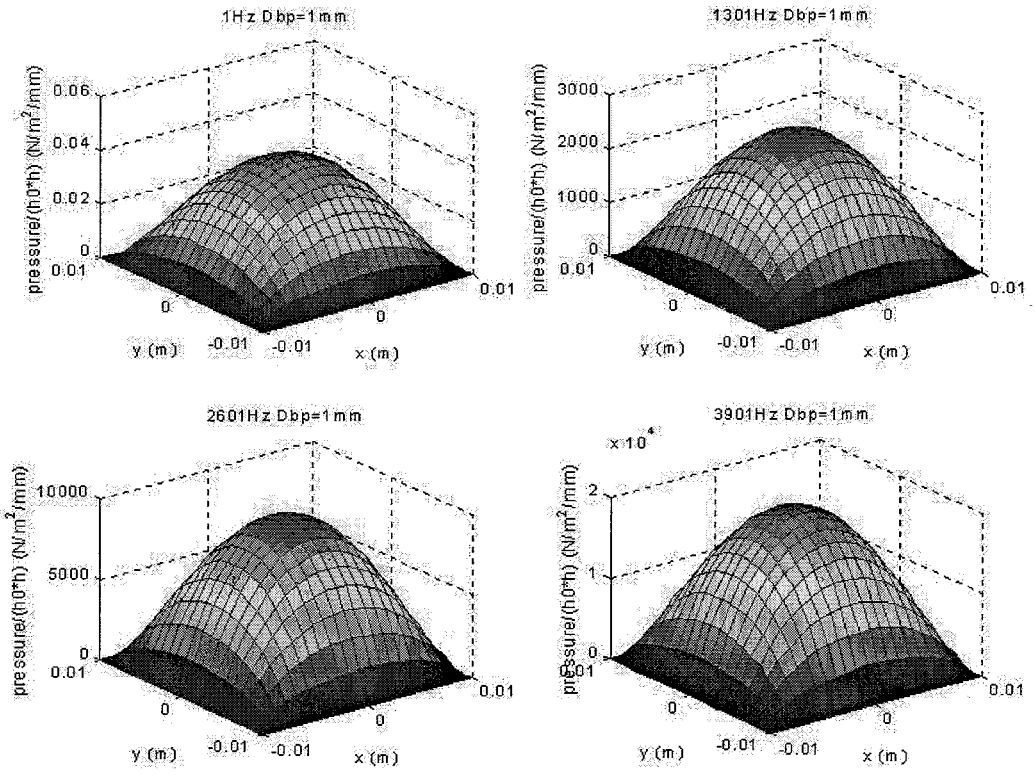

*Figure 4.3: Pressure distribution/amplitude: lx=10, ly=10, 2*h0=1 mm*

It can be concluded that the low reduced frequency model can be used if the amplitude of the tread is not to small, because otherwise the boundary condition of p=0 is not valid anymore. In appendix G this conclusion is confirmed using model B, which will be discussed in chapter 5.

4.4: Results

It is important to define interesting parameters for the whole region of the tyre/road noise problem to produce interesting results.

1) *Size vibrating patch*
   The size of the vibrating patch must be of the same size as the blocks of a normal tread. It is chosen to study 2 sizes: 10x10mm and 20x20mm.
2) *Size gap*
   The model is valid up to gap sizes with a maximum of 5-10 mm, so values between 0 and 10 are chosen: 0.1mm, 0.5mm, 1mm, 2mm, 5mm and 10mm.
3) *Amplitude*
   The amplitude of the tyre tread is hard to determine. "Assuming small amplitudes" it is chosen to normalize the pressure and the force using the amplitude, so later on it is easy to determine the pressure and force if the amplitude is known from further research.
4) *Frequency*
   For the frequency the range 0-4000 Hz is chosen (see 4.3).

Now for each size of the tread block the force and the eigenfrequency plot will be shown. For the calculation of the eigenfrequencies the data for the mass and stiffness of the springs from [8] are used. In this report the tread block is supported with 2 springs that each have a stiffness of 6.946 10^4 N/m. The mass of the tread block is 3.63 10^{-4} kg. This is of course only general data, but it is good enough to get an idea of the effects on a "real" tyre tread block.

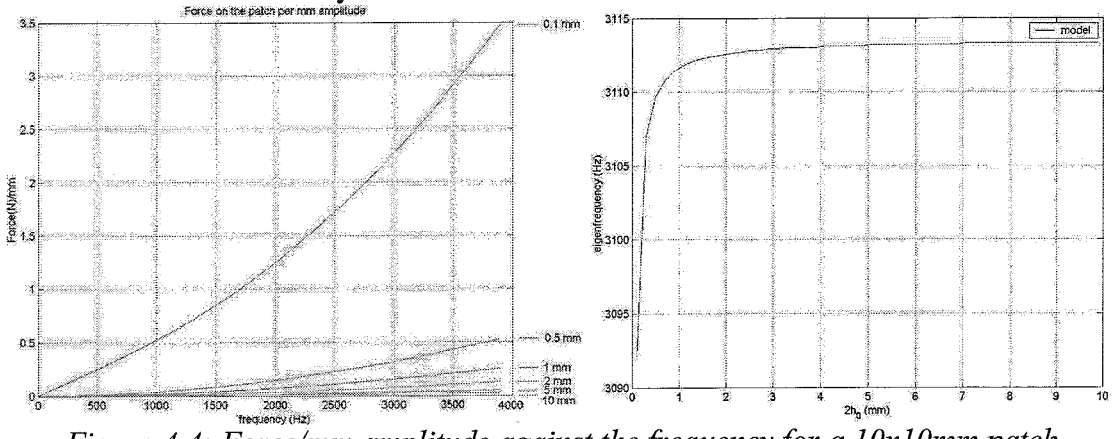

Figure 4.4: Force/mm amplitude against the frequency for a 10x10mm patch The gap varies between 0.1mm and 10mm. The smallest gap gives the highest force. The eigenfrequency of the 10x10mm patch plotted against the gap size. (eigenfrequency from FE calculation with the same parameters: 3113.6Hz [8])

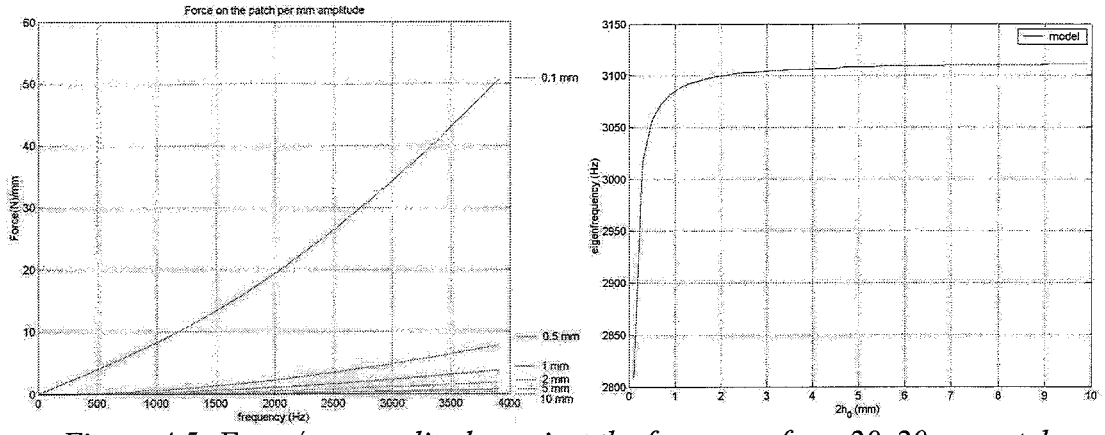

Figure 4.5: Force/mm amplitude against the frequency for a 20x20mm patch The gap varies between 0.1mm and 10mm. The smallest gap gives the highest force. The eigenfrequency of the 20x20mm patch plotted against the gap size. (eigenfrequency from FE calculation with the same parameters: 3113.6Hz [8])

For the tyre tread block of 20mm x 20mm a plot is made that shows the transfer function for 3 different heights.

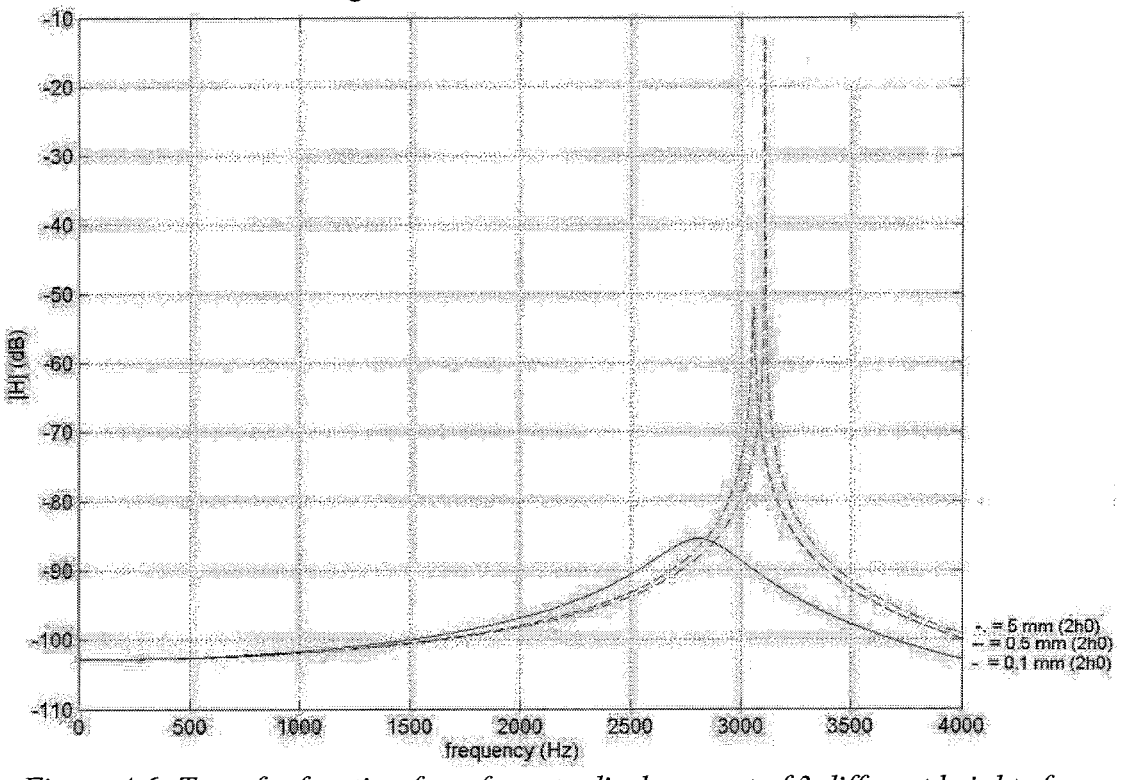

Figure 4.6: Transfer function from force to displacement of 3 different heights for a patch of 20x20mm. The smaller the gap, the more eigenfrequency changes. (dB re 1 N)

In figure 4.6 and 4.5 part two an eigenfrequency around the 3000 Hz is shown, but this eigenfrequency is not visible in part one of figure 4.5. This is because the input in part one of figure 4.5 is constant over the whole frequency range, which means that the mass-spring system properties are not taken into account in this figure.

4.5: General conclusions

The first conclusion is that the eigenfrequency decreases with decreasing gap size and that this effect increases with an increasing patch size. The explanation for this is that the air in the gap acts like an "added" mass, so the eigenfrequency (the eigenfrequency of a mass-spring system: $f_0 \sim \sqrt{k/m}$) will decrease. The second conclusion is that the transfer function is more damped if the gap size decreases. This is due to the extra damping added by the increased viscous and thermal effects in the air. The third conclusion is that the force increases rapidly if the gap sizes get smaller for given amplitude. The force is plotted in the graphs as N/mm. To make real conclusions about the force the amplitude of a tyre tread block should be known. At this moment there is no measured data available of the amplitude of a rubber block due to adhesion, because it is difficult to measure the adhesion, because it is hard to mount the transducers near the contact where the adhesion force acts. There are measurements available from tyres, but in these measurements the effect of the air layer is included, so it is difficult to extract from these experiments what size the amplitude would be without the air.

At the end of the layer there is no pressure perturbation due to the boundary condition p=0. It would have been useful to rewrite the formulas to include an end-impedance ("pressure divided by velocity" at the edges), but there are two problems with this approach. First to find a good end-impedance, because of the non-linear pressure profile and second the whole formula is based around the assumption of p=0 and so the whole formula must be formulated at a different way.

It has been proven in this chapter that the model is a powerful tool to study a part of the air-effect on the tyre/road noise problem.

Chapter 5: Model B: a patch vibrating in a tube

The model that will be developed in this chapter can predict the forces on a patch vibrating inside a tube and it can predict the far field sound in free air. This model can be used to simulate the vibration of the walls in tyre grooves. The formulas for a tube from the low reduced frequency model (appendix C) are used to develop this model, but also a paper from Tijdeman [5] and the book Theoretical Acoustics (1968) [6] are used for this problem.

5.1: Model

The model looks like this:

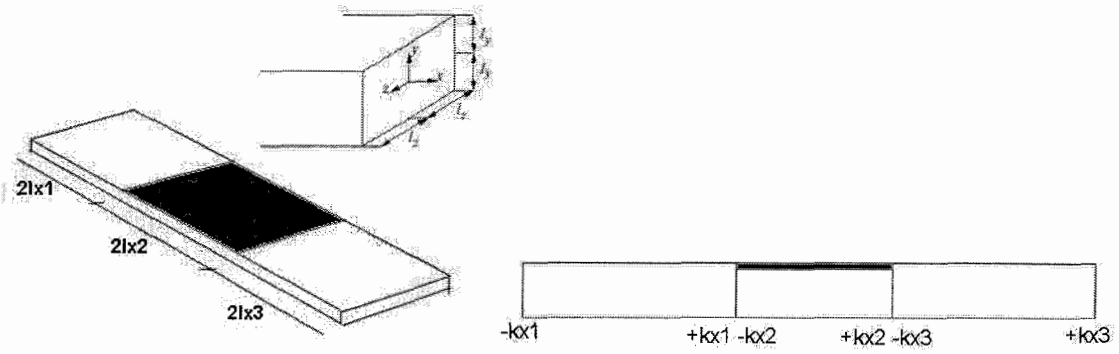

Figure 5.1: 3 parts coupled; with dimension and dimensionless

The tube is divided in three parts as can be seen in figure 5.1. For the part with a vibrating patch and for the parts without vibrating patch there is a separate calculation of the pressure with the low reduced frequency model.
First the dimensionless parameters are defined:

$$kx_1 = \frac{lx_1 \cdot \omega}{c_0} \tag{27}$$

$$kx_2 = \frac{lx_2 \cdot \omega}{c_0} \tag{28}$$

$$kx_3 = \frac{lx_3 \cdot \omega}{c_0} \tag{29}$$

The basic formula is formulated as (chapter 3):

$$\Delta^{pd} P(x^{pd}) - k^2 \Gamma^2 p(x^{pd}) = -ikn(s\sigma)\Gamma^2 \Re \tag{16}$$

It is assumed that the pressure only depends on the x coordinate [1]. The velocity depends on all the coordinates, because:

$$v^{pd}(s, x^{pd}, x^{cd}) = \frac{-i}{k\gamma} A(s, x^{cd}) \nabla^{pd} p(x^{cd}) \tag{30}$$

$$\nabla^{pd} = e_x k \frac{\partial}{\partial x} \tag{31}$$

For the tubes the basic equations are:

$$\frac{\partial^2 p}{\partial x^2} - \Gamma^2 p = \frac{1}{2} n(s\sigma)\Gamma^2 L \tag{32}$$

$$\frac{\partial^2 p}{\partial x^2} - \Gamma^2 p = 0 \tag{33}$$

where (32) is for the part with one vibrating patch (L is dimensionless amplitude of the patch $\overline{L} = L_o(2 + Le^{i\omega t})$) and formula 33 is for the parts without vibrating patch. The exact derivation of the formulas is shown in appendix C.

For both a solution of the pressure must be found. From the literature [1] and [6] it is concluded that a standard solution for the pressure for a tube without vibrating patch is of the form:

$$p = Ae^{-\Gamma x} + Be^{\Gamma x} \tag{34}$$

In this solution one-dimensional wave propagation with one wave traveling from left to right and one vice versa are included. For the part with vibrating patch an extra factor is added to the basic formula (34) to make it fit to (32). This results in the next three formulas are available for the different parts:

$$p_1 = -A_1 e^{-\Gamma x} + A_2 e^{\Gamma x} \tag{35}$$

$$p_2 = -B_1 e^{-\Gamma x} + B_2 e^{\Gamma x} - \frac{1}{2} n(s\sigma)L \tag{36}$$

$$p_3 = -C_1 e^{-\Gamma x} + C_2 e^{\Gamma x} \tag{37}$$

Together there are six unknown variables in the equation: A1,A2,B1,B2,C1 and C2. But two extra unknowns, p_{x1} and p_{x2}; the pressures at the coupling point, are introduced by the fact that the parts are coupled together. So in total there are eight unknowns, which means that eight boundary conditions are needed.

1) $p_0 p_1(-k_{x1})/c_0 v_1(-k_{x1}) = Z$ for an open end. (38)
   $v_1(-k_{x1}) = 0$ for a closed end. (39)
2) $p_1(k_{x1}) = p_{x1}$ (40)
3) $p_2(-k_{x2}) = p_{x1}$ (41)
4) $p_2(k_{x2}) = p_{x2}$ (42)
5) $p_3(-k_{x3}) = p_{x2}$ (43)
6) $p_0 p_3(k_{x3})/c_0 v_3(k_{x3}) = Z$ (44)
7) $S1 * v_1(k_{x1}) = S2 * v_2(-k_{x2})$ (45)
8) $S2 * v_2(k_{x2}) = S3 * v_3(-k_{x3})$ (46)

Where S1, S2 and S3 are the cross-section areas of the tubes and Z is the end-impedance. Formula (45) reduced to $\frac{\partial p_1}{\partial x} = \frac{\partial p_2}{\partial x}$ and (46) reduces to $\frac{\partial p_2}{\partial x} = \frac{\partial p_3}{\partial x}$ if the tubes have the same cross-section area. In (38) and (44) Z is the same, but the sign is different, which is because the velocity changes sign. Also the dimensionless pressure is multiplied by p_0 and the dimensionless speed by c_0. This is necessary, because the end-impedance is based on real pressures and real velocities.

With these conditions a basic A*b=C system can be set up to determine the value of the variables. It must be mentioned that these values are all frequency dependent.

If $p_3(k_{x3}) = 0$ and $p_1(-k_{x1}) = 0$, so if it is assumed that the pressure is zero at the beginning and end of the tube, then the following equation follows:

$$\begin{bmatrix} -e^{\Gamma kx_1} & e^{-\Gamma kx_1} & 0 & 0 & 0 & 0 & 0 & 0 \\ -e^{-\Gamma kx_1} & e^{-\Gamma kx_1} & 0 & 0 & 0 & 0 & -1 & 0 \\ 0 & 0 & -e^{\Gamma kx_2} & e^{-\Gamma kx_2} & 0 & 0 & -1 & 0 \\ 0 & 0 & -e^{-\Gamma kx_2} & e^{\Gamma kx_2} & 0 & 0 & 0 & -1 \\ 0 & 0 & 0 & 0 & -e^{\Gamma kx_3} & e^{-\Gamma kx_3} & 0 & -1 \\ 0 & 0 & 0 & 0 & -e^{-\Gamma kx_3} & e^{\Gamma kx_3} & 0 & 0 \\ \Gamma e^{-\Gamma kx_1} & \Gamma e^{\Gamma kx_1} & -\Gamma e^{\Gamma kx_2} & -\Gamma e^{-\Gamma kx_2} & 0 & 0 & 0 & 0 \\ 0 & 0 & \Gamma e^{-\Gamma kx_2} & \Gamma e^{\Gamma kx_2} & -\Gamma e^{\Gamma kx_3} & -\Gamma e^{-\Gamma kx_3} & 0 & 0 \end{bmatrix} \cdot \begin{bmatrix} A_1 \\ A_2 \\ B_1 \\ B_2 \\ C_1 \\ C_2 \\ p_{x1} \\ p_{x2} \end{bmatrix} = \begin{bmatrix} 0 \\ 0 \\ \frac{1}{2} n(s\sigma)L \\ \frac{1}{2} n(s\sigma)L \\ 0 \\ 0 \\ 0 \\ 0 \end{bmatrix} \quad (47)$$

Of course it is possible for "easy" boundary conditions ($p_1(-k_{x1})=0$ and $p3(k_{x3})=0$) to solve the problem analytically. The procedure for this is shown in Appendix D. For more difficult boundary conditions (with end-impedances etc) it becomes a lot more work to solve it analytical. It is beyond this report to look at that complicated time consuming analytical solutions.
For the system with two open ends the next A*b=C system is used to calculate the values of the variables:

$$\begin{bmatrix} X1 & X2 & 0 & 0 & 0 & 0 & 0 & 0 \\ -e^{-\Gamma kx_1} & e^{-\Gamma kx_1} & 0 & 0 & 0 & 0 & -1 & 0 \\ 0 & 0 & -e^{\Gamma kx_2} & e^{-\Gamma kx_2} & 0 & 0 & -1 & 0 \\ 0 & 0 & -e^{-\Gamma kx_2} & e^{\Gamma kx_2} & 0 & 0 & 0 & -1 \\ 0 & 0 & 0 & 0 & -e^{\Gamma kx_3} & e^{-\Gamma kx_3} & 0 & -1 \\ 0 & 0 & 0 & 0 & X3 & X4 & 0 & 0 \\ \Gamma e^{-\Gamma kx_1} & \Gamma e^{\Gamma kx_1} & -\Gamma e^{\Gamma kx_2} & -\Gamma e^{-\Gamma kx_2} & 0 & 0 & 0 & 0 \\ 0 & 0 & \Gamma e^{-\Gamma kx_2} & \Gamma e^{\Gamma kx_2} & -\Gamma e^{\Gamma kx_3} & -\Gamma e^{-\Gamma kx_3} & 0 & 0 \end{bmatrix} \cdot \begin{bmatrix} A_1 \\ A_2 \\ B_1 \\ B_2 \\ C_1 \\ C_2 \\ p_{x1} \\ p_{x2} \end{bmatrix} = \begin{bmatrix} 0 \\ 0 \\ \frac{1}{2} n(s\sigma)L \\ \frac{1}{2} n(s\sigma)L \\ 0 \\ 0 \\ 0 \\ 0 \end{bmatrix} \quad (48)$$

$$X1 = -p_0 e^{\Gamma kx_1} - c_0 Z \cdot \frac{i}{\gamma} \cdot A(s) \cdot \Gamma \cdot e^{\Gamma kx_1} \quad (49)$$

$$X2 = p_0 e^{-\Gamma kx_1} - c_0 Z \cdot \frac{i}{\gamma} \cdot A(s) \cdot \Gamma \cdot e^{-\Gamma kx_1} \quad (50)$$

$$X3 = -p_0 e^{-\Gamma kx_3} + c_0 Z \cdot \frac{i}{\gamma} \cdot A(s) \cdot \Gamma \cdot e^{-\Gamma kx_3} \quad (51)$$

$$X4 = p_0 e^{\Gamma kx_3} + c_0 Z \cdot \frac{i}{\gamma} \cdot A(s) \cdot \Gamma \cdot e^{\Gamma kx_3} \quad (52)$$

For the system with one open end and one closed end the following system is used to calculate the values of the variables:

$$\begin{bmatrix} \Gamma \cdot e^{\Gamma kx_1} & \Gamma \cdot e^{-\Gamma kx_1} & 0 & 0 & 0 & 0 & 0 & 0 \\ -e^{-\Gamma kx_1} & e^{-\Gamma kx_1} & 0 & 0 & 0 & 0 & -1 & 0 \\ 0 & 0 & -e^{\Gamma kx_2} & e^{-\Gamma kx_2} & 0 & 0 & -1 & 0 \\ 0 & 0 & -e^{-\Gamma kx_2} & e^{\Gamma kx_2} & 0 & 0 & 0 & -1 \\ 0 & 0 & 0 & 0 & -e^{\Gamma kx_3} & e^{-\Gamma kx_3} & 0 & -1 \\ 0 & 0 & 0 & 0 & X3 & X4 & 0 & 0 \\ \Gamma e^{-\Gamma kx_1} & \Gamma e^{\Gamma kx_1} & -\Gamma e^{\Gamma kx_2} & -\Gamma e^{-\Gamma kx_2} & 0 & 0 & 0 & 0 \\ 0 & 0 & \Gamma e^{-\Gamma kx_2} & \Gamma e^{\Gamma kx_2} & -\Gamma e^{\Gamma kx_3} & -\Gamma e^{-\Gamma kx_3} & 0 & 0 \end{bmatrix} \cdot \begin{bmatrix} A_1 \\ A_2 \\ B_1 \\ B_2 \\ C_1 \\ C_2 \\ p_{x1} \\ p_{x2} \end{bmatrix} = \begin{bmatrix} 0 \\ 0 \\ \frac{1}{2} n(s\sigma)L \\ \frac{1}{2} n(s\sigma)L \\ 0 \\ 0 \\ 0 \\ 0 \end{bmatrix} \quad (53)$$

5.2: End-Impedance

As can be seen in the defined systems there is one unknown extra in the matrix called Z. This is a function that describes how the pressure divided by velocity is defined at

the end of the tube(s). It is interesting to implement an end-impedance, because it is then possible to calculate a velocity and pressure at the ends of the tube, so it is possible to say something about the radiated sound from the tube. Another benefit is that the predicted pressure inside the tube will be more accurate. The expression for Z for an end-impedance of a tube with a rectangular cross-section will be discussed in this report.
First it is important to say that the open tube end will be simulated with a driving piston. This is valid for the long-wavelength limit [5] in which the wavelength is long compared to the contour of the tube. The wavelength at 3000 Hz is 0.114 m. So if the tube has a cross-section with sides of 5 mm than the contour is 0.02m and so it can be conclude that the long-wavelength limit is valid in the cases that are studied in this report.
Also the velocity profile is checked to look if the approximation of a piston makes sense. The velocity profile is completely determined by the dimensionless function A [1], so the function A is plotted for the dimensionless values of z and y for a square tube cross-section. As can be seen in figure 5.2 the velocity is almost constant over the whole area of the tube, so it seems that the use of a piston is a valid approximation for the frequencies of 100 Hz and higher.

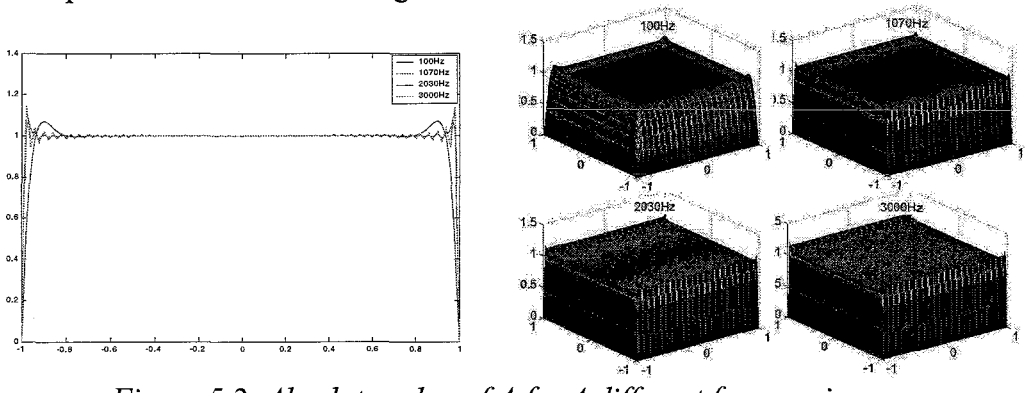

Figure 5.2: Absolute value of A for 4 different frequencies

5.2.1: End-impedance of a tube with rectangular cross-section

As said before the piston impedance will simulate the end of the tube. In the literature ([6] and [7]) the impedance of a flanged piston is described. This is the impedance of a piston moving in an infinite plate, which is the best approximation in this case. This is because a tube in free space is even less comparable to the profile (tube) ending at the wall of the tyre.
In the literature ([6] and [7]) the radiation impedance of a piston, which is the force on the piston divided by the velocity, can be found. For this research the pressure divided by the velocity is required. This is achieved by dividing the radiation impedance with the area of the piston. This can be done, because the pressure in the model is almost constant over the whole area (one of the assumptions of the low reduced frequency model; chapter 4).
The dimensions used in the formula for the tube with rectangular cross-section are a and b. These are the lengths of the sides of the piston. Two different impedances are found. One impedance is valid if b is about the same size as a (case one). The second one is valid as long as a/b is neither very large nor very small (case two).

$$Z_r = \rho cab[\theta_0(ka) - iX_0(ka)] \text{ for case 1} \qquad (54)$$

$$Z_r = \rho cab \frac{a^2\theta_0(ka) - b^2\theta_0(kb) - ia^2 X_0(ka) + ib^2 X_0(ka)}{a^2 - b^2} \quad \text{for case 2} \qquad (55)$$

$$\theta_0(z) = \left[1 - 4\frac{1 - J_0(z)}{z^2}\right] \qquad (56)$$

$$X_0(z) = \frac{8}{\pi z}\left[1 - \frac{\pi}{2z} M_0(z)\right] \qquad (57)$$

$$k = \frac{\omega}{c} \qquad (58)$$

where J_0 is the Bessel function of the zero order and M_0 is the Struve function of the zero order.
The Z that will be used in this report is Z_r defined by (54) or (55) divided by the area of the tube, which is *ab*.

In figure 5.3 an example of the impedance and the reflection factor is given.
The reflection factor is defined as the impedance minus the impedance of a plane wave in free air ($\rho_0 c_0$) divided by the impedance plus the impedance of a plane wave in free air.

$$\text{Reflection factor} = \frac{Z - \rho_0 c_0}{Z + \rho_0 c_0} \qquad (59)$$

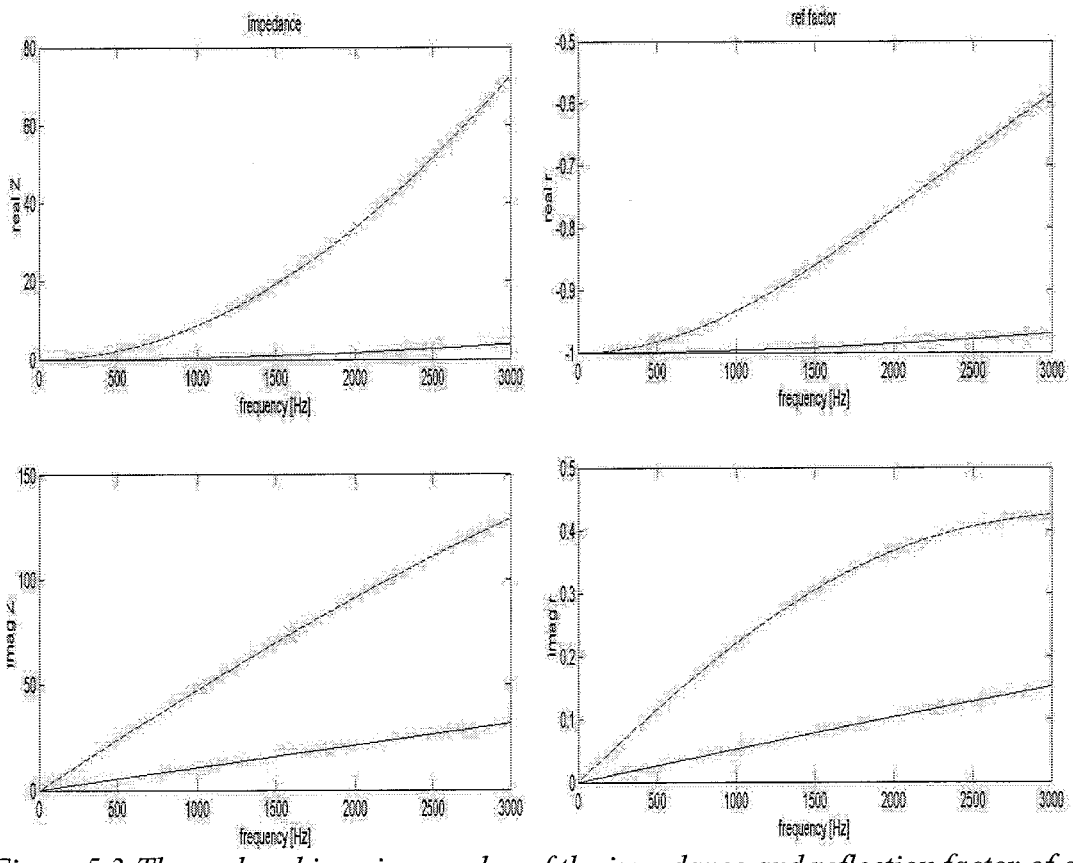

Figure 5.3: The real and imaginary value of the impedance and reflection factor of an opening of 10x10mm (-) and of an opening of 10x30mm(--)

The conclusion from the figures is that there is not that much leakage of air if the opening is small, because the reflection factor is close to –1. This implies that the end-impedance of the opening is very small (near zero), which implies that the boundary

condition of p=0 could be valid too. However if the opening gets larger the reflection factor gets smaller, so the end-impedance of the tube has an effect on the pressure distribution in the tube, so for small amplitudes in combination with large gaps p=0 is not a valid boundary condition. This is the reason why the end-impedance Z will be used for the calculations in this report.

5.2.2: Bessel and Struve function

In the impedance functions of a rectangular opening Bessel and Struve functions are used. The Bessel function is a function that is implemented in Matlab, so implementing this in the m-file is straightforward. The Struve function is not implemented in Matlab (R12).
The Struve function of zero order is defined as in [6]:

$$M_0(z) = \frac{2}{\pi}\int_0^{\pi/2} \sin(z\cos(u))du \tag{60}$$

The analytical Struve function is solved in 2 different ways:

1) With a for loop in Matlab (iterative)
2) With external m-file from the internet ([10])

In the calculations in this report the external m-file is used, because it needs the least calculation time.

5.2.3: Implementation of end-impedance to the model

Before implementing the end-impedance in the model it is important to look if it can be implemented straightforward from the book.

Model:
In the model the real pressure variation and velocity are defined as:

$$\overline{v} = c_0 v e^{i\omega t} \tag{5}$$

$$\overline{p} = p_0 p e^{i\omega t} \tag{61}$$

And the dimensionless pressure in tube 1 and 3 is defined as:

$$p_3 = -C_1 e^{-\Gamma x} + C_2 e^{\Gamma x} \tag{62}$$

Because Γ has an imaginary part / is purely imaginary it is possible to write the real pressure variation in the next way:

$$\overline{p} = Ae^{-jkx}e^{j\omega t} + Be^{jkx}e^{j\omega t} \tag{63}$$

Where the first part will be called p_{+B} and the second part will be called p_{-B}.
The velocity function is *defined* as:

$$\frac{\partial u}{\partial t} = -\frac{1}{\rho}\frac{\partial p}{\partial x} \tag{64}$$

For small oscillations this can be rewritten as:

$$u = \frac{1}{-j\omega\rho}\frac{\partial p}{\partial x}\text{ , so} \tag{65}$$

$$u = \frac{1}{-j\omega\rho}(-jkp_{+B} + jkp_{-B}) \tag{66}$$

Now it can be stated that the impedance is of a general form a+jb, so:

$$Z = a + jb = \frac{p_{+B} + p_{-B}}{\frac{1}{-j\omega\rho}(-jkp_{+B} + jkp_{-B})} \tag{67}$$

The can be rewritten as:

$$Z = \rho c_0 \frac{p_{+B} + p_{-B}}{(p_{+B} - p_{-B})} \text{ for} \tag{68}$$

Theoretical Acoustics [6]:
In the book the pressure is defined as:

$$\bar{p} = Ae^{jkx}e^{-j\omega t} + Be^{-jkx}e^{-j\omega t} \tag{69}$$

Where the first part will be called p_{+T} and the second part will be called p_{-T}.
The velocity in the book is *defined* as:

$$u = \frac{1}{j\omega\rho}(jkp_{+T} - jkp_{-T}) \tag{70}$$

Now can be stated that the impedance is:

$$\frac{p_{+T} + p_{-T}}{\frac{1}{j\omega\rho}(jkp_{+T} - jkp_{-T})} \tag{71}$$

This can be rewritten as:

$$Z = \rho c_0 \frac{p_{+T} + p_{-T}}{(p_{+T} - jkp_{-T})} \text{ for} \tag{72}$$

Comparison:
From the two formulas for the pressure it can be concluded that $p_{+B} = p_{+T}^*$ and $p_{+B} = p_{-T}^*$. Now it can be concluded that both formulas are of the same form, but that they are the complex conjugate of each other. So the complex conjugate of the impedance found in the book Theoretical Acoustics [6] has to be taken for the model.

5.3: Far field pressure

To look at the sound pressure at a certain distance at a certain angle, it is not enough to just know the pressure and velocity at the end of the tube. It is necessary to include a formula for the far field noise. The far field noise equation for a rectangular piston is found in [6] and is defined as:

$$p_\omega(r) = 2ik\rho c u_w abS(\frac{1}{2}ka\sin(\vartheta)\cos(\varphi))S(\frac{1}{2}kb\sin(\vartheta)\sin(\varphi))\frac{e^{ikr}}{4\pi r} \tag{73}$$

where S(z) is sin(z) divided by z, ϑ is the vertical angle between the normal line through the piston and the position of the receiver, φ is the horizontal angle between the normal line through the piston and the position of the receiver, k is the frequency in rad/s divided by the speed of sound and a and b are the dimensions of the rectangular.

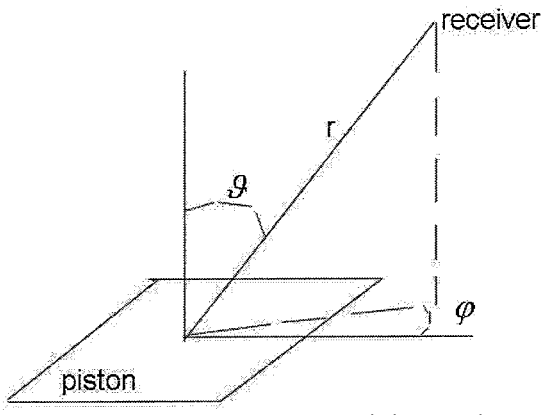

Figure 5.4: Definition of the angles

Again for the same reason as mentioned before with the implementation of the end-impedance the complex conjugate of the far field pressure found in the book Theoretical Acoustics [6] must be implemented in the model.

5.4: Experimental Setup

To validate the model an experiment is performed. The idea is to do measurements with only two different tubes of plexiglas. The two tubes have both the same vibrating patch, so part two is of the same length in both cases, but the other parts are different. To measure great effects and to be able to construct the tubes quite easy the next dimensions are chosen:

Table 1

	Length part 1	*Length part 2*	*Length part 3*	*Width*	*Heigth*
Tube 1	100 mm	60 mm	100 mm	20 mm	11, 16 or 21 mm
Tube 2	150 mm	60 mm	150 mm	20 mm	11, 16 or 21 mm

2 Accelerometers (Deltashear/Briiel & Kjaer type 4393V; sensitivity 0.316 pC/ms^2, 0.1-16500Hz and 2.4 grams each) are mounted on the patch to measure the acceleration. The patch is driven by a shaker (LDS V406), which is attached to the patch with glue. The patch is a bit smaller than the gap in the tube to avoid friction forces. A rubber sealing is added between/on top of the patch-tube connection to avoid air-leakage. 7 Microphones are inserted in a wall of the tube of 360 mm to measure the sound pressure on 7 different places: 2,4,6,8,10,12 and 14 mm from the opening of the tube. Also a microphone is added just in front of the opening (5mm) to measure the pressure at the end of the tube. The microphones are calibrated using a calibration tool that has a fixed sound pressure level at 1000 Hz (Briiel & Kjaer Type 4231). In total 2 sound pressures can be measured at the same time but it is possible to switch between the microphones with a switch box. The far field noise in a free environment is not measured, because the conditions are not good enough (surrounding noise of the shaker and the computer). Another problem is that the tube has two openings, so if the far field noise is measured at a point it is a combination of those two.

The output signal of the computer is amplified with a power amplifier (LDS PA100E). The input signal of the accelerometers is amplified and conditioned with a conditioning amplifier of Briiel & Kjaer. The computer unit that is used consists of a Hewlett Packard ICP/voltage 8ch input, Agilent E8408AVXI Mainframe and a Netwerver LPr. The output signal is made with the program Triggerhappy v1.0 and

this program is also used to read the input signals (1x output, 2x accelerometers, 2x microphone). The data processing is performed with Matlab R12.

Schematic overview of the setup:

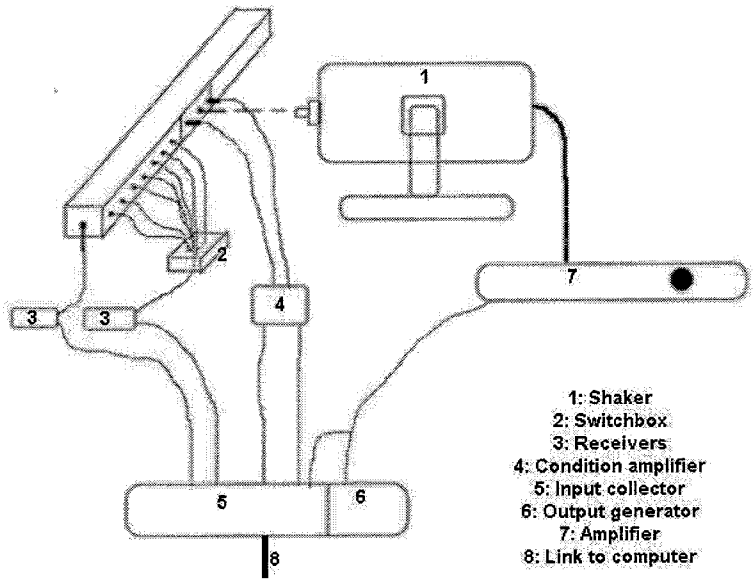

Figure 5.5: Schematic overview setup

Photos of the setup:

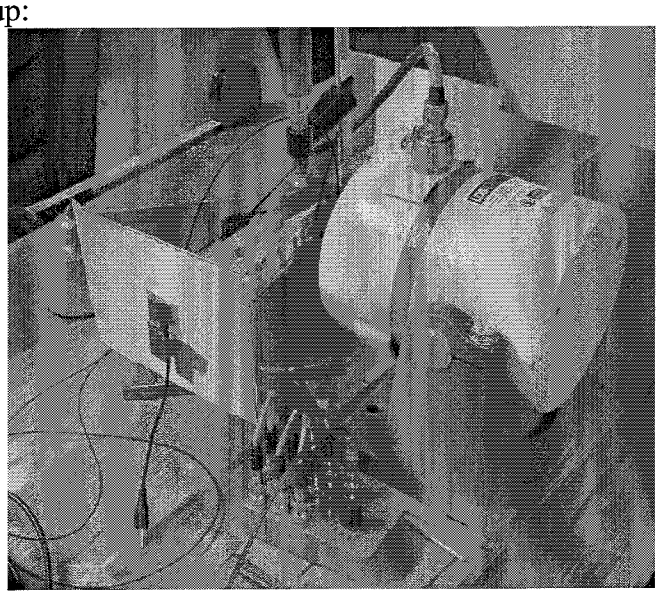

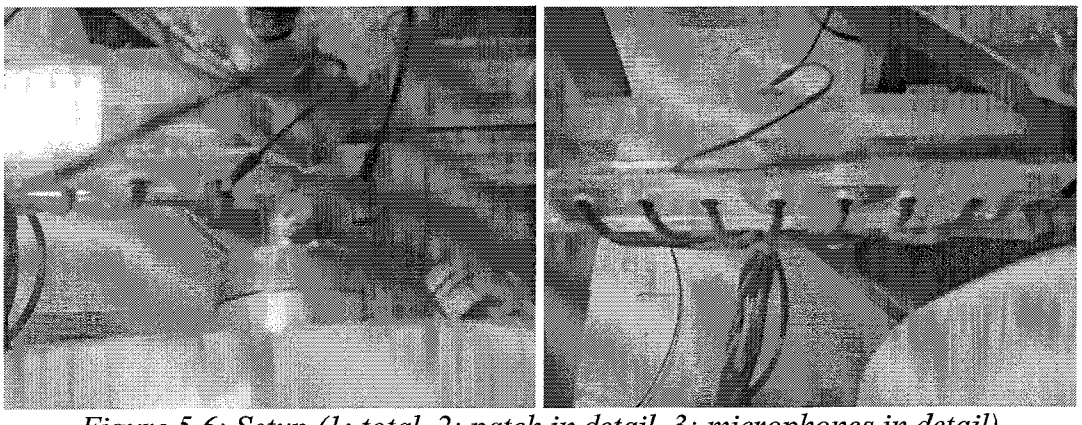

Figure 5.6: Setup (1: total, 2: patch in detail, 3: microphones in detail)

5.5: Experimental Results – Results model

The transfer function, where the output is the pressure and input is the acceleration, of the tube is measured using a random signal. After some measurements at different frequencies the conclusion is that above 2500 Hz the patch does not vibrate in phase anymore. One accelerometer gives a high value and the other one a low value. This is the reason why only measurements until 2500 Hz are performed.

5.5.1: Transfer function

In the model the transfer function is made using a sinusoidal signal as input.
In the experiments there are some extra peaks in the transfer function at certain frequencies. If a measurement is performed with a sinusoidal signal at these frequencies the high levels do not show up. If the voltage level of the random signal is lowered the peaks are clearer visible and if the voltage is increased the peaks become less dominant. The coherence between the input (the shaker) and the accelerometers is checked and at the frequencies of the "strange" peaks there is a large coherence dip. This has two different reasons. The first is that there is a strange crackling/rattling noise at the vibrating patch, which causes problems. The second is that the patch does not vibrate with the entire surface in one phase.
A difference in level between the plots of the transfer function that is measured or the transfer function from the model by calculating the acceleration at the whole frequency range with steps of 1 Hz is clearly visible. However if a measurement is performed with a sinusoidal signal then the levels of both plots are the same.
For these reasons it is decided only to look at the differences between the frequencies of the peaks of the model and the experiment.

First an experiment with the tube of 360 mm length is performed. The height of the tube is 11mm, because the lower the height the lower k and k/s (see 4.3.1), so the more reliable the model.

Experiment:

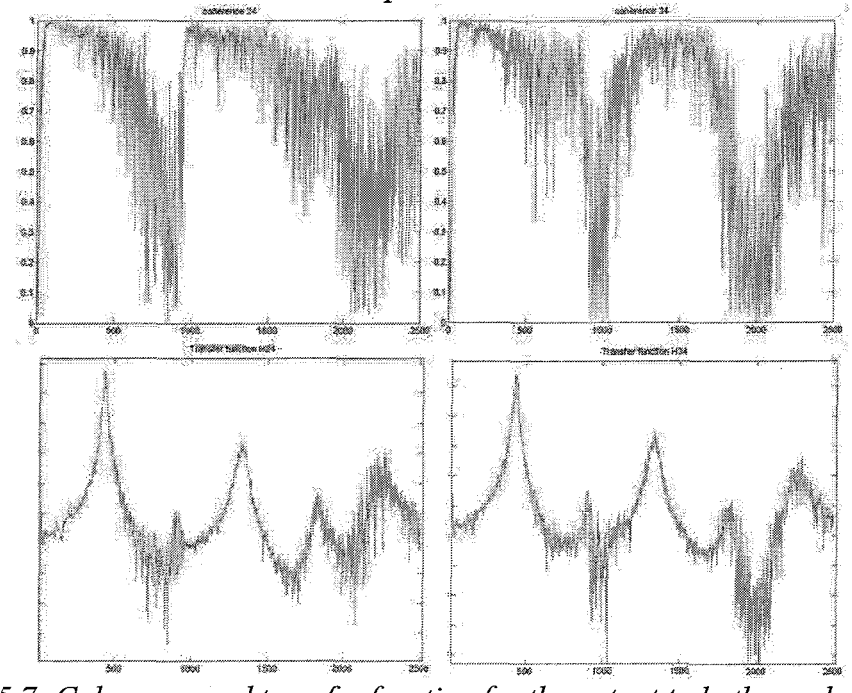

Figure 5.7: Coherence and transfer function for the output to both accelerometers

From figure 5.7 it can be concluded that there are 3 peaks around the 500, 1400 and 2300 Hz that show up in both figures and have about the same size. The coherence is reasonable at those peaks, so that means that the results can be trusted. What also can be concluded from the figures is that the peaks around 800 and 2000 Hz do not have the same amplitudes in both figures, so for each accelerometer the effect at those frequencies is different, although the amplitudes at the "eigenfrequencies" of the tube are the same. Also the coherence is bad, so that is the reason why only the three peaks around 500, 1400 and 2300 Hz are trusted. A final remark is that the 2300 Hz peak is not that clear as the 500 Hz and the 1400 Hz peak. However the peak at 2300 Hz is considered to be good enough to use in the comparison.

Model:

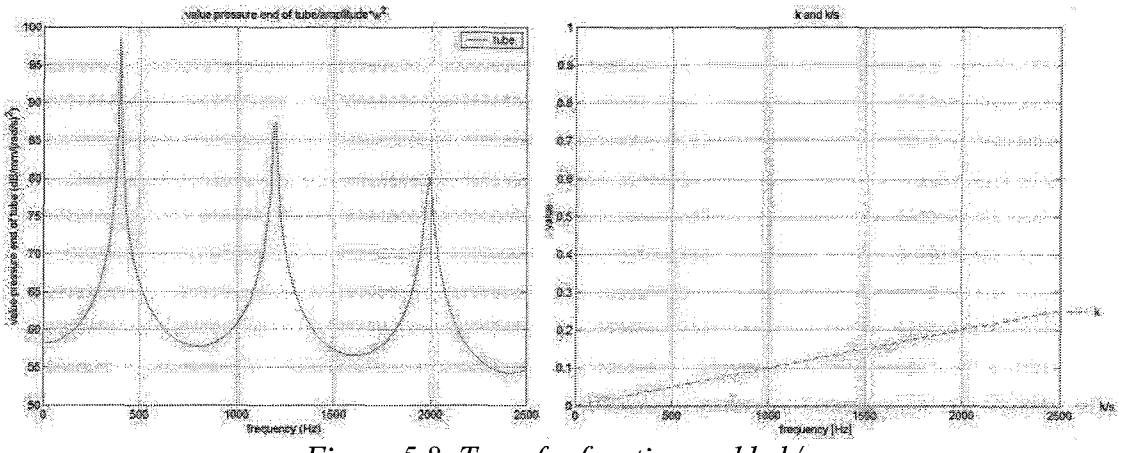

Figure 5.8: Transfer function and k, k/s

The input for the model is the amplitude in meters of the patch and the output is the pressure. The input in the experiments is the acceleration, so the "original" transfer function of the model is divided by ω^2, which is the factor between the second derivate and the original of a sinusoidal function.

Comparison:

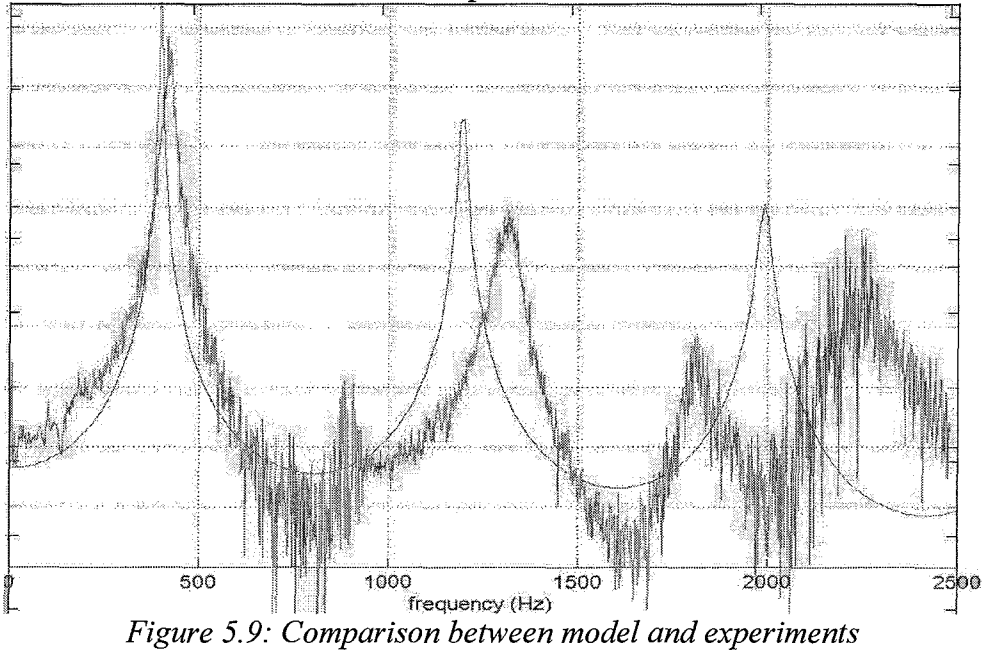

Figure 5.9: Comparison between model and experiments

From figure 5.9 it can be concludes that the shape of the figure is the same, but that there is a large difference in the value of the eigenfrequencies.

Table 2:

	Model ([Hz])	Experiment ([Hz])	Difference ([%])
Eigenfrequency 1	382	430	12.5
Eigenfrequency 2	1147	1335	16.4
Eigenfrequency 3	1912	2250	17.6

Over the whole frequency range there is a difference of about 15 %.
The same conclusion can be drawn for the tube of 240 mm.

Table 3:

	Model ([Hz])	Experiment ([Hz])	Difference ([%])
Eigenfrequency 1	530	618	16.6
Eigenfrequency 2	1580	1840	16.4

Over the whole frequency range there is a difference of about 16 %.
The difference for both tubes is around the 15-16%, which is quite large and that is the reason why all the variables in the model are checked.
It appeared the function B (19), as given in [1], does not convert to –1 for high values of the shear wave number but to –0.74. It would be expected that the value goes to –1, because:

- It is stated in [1] and appendix D that "B" should go to –1 for high shear wave numbers.
- "B" is defined as: $B(s) = \frac{1}{A^{cd}} \int_{A^{cd}} A(s, x^{cd}) dA^{cd}$ (19)

  It is known from earlier calculations that "A" is –1 (absolute value is 1) over almost the whole area, because the piston approximation is based upon this. If "A" is seen as a constant it is easy to conclude from (19) that "B" is also -1.
- By numeritical integration of "A" over the whole area and than dividing by the area the function converts to –1 for high shear wave numbers.
- The value of "B" of a tube with a circular cross-section [1] also goes to –1 for high shear wave numbers.

It can be concluded that very strong indications are available that the B function as stated in [1] is wrong. In appendix F calculations are performed with a "corrected" "B" and in these calculations a better match is achieved between the model and the experiments.
However in this report the calculations will be performed with the "B" from [1], because this is a "B" that is published. Despite the strong indications that this "B" is wrong, it is unclear what is a good "B", because there are no publications known about how the A and B functions are determined in [1] and so it was impossible to find the "correct" values.
If it would be proven later that the "B" function found in [1] is wrong than the only thing that would differ are the frequencies, because the levels that are predicted with the "B" found in [1] and the "correct" "B" are the same at the same places on both the curves (for example around the "same" eigenfrequency peak). So the conclusions stated in this report would remain the same.

5.5.2: Sound-pressure in tube

This measurement is only performed with the tube of 360 mm, because this is the only tube with microphones. To make a good comparison between the experiment and the model a frequency shift is adapted. This frequency shift is necessary because the frequencies of the peaks are about 15 % different (table 2 and 3). To make a fair comparison there is a factor 1.15 introduced (frequency model * 1.15=frequency measurement). So if the experiment is performed at 2000 Hz, the calculation in the model is performed at 1740 Hz (2000/1.15). This shift is necessary, because it could be possible that the measurement is made at the eigenfrequency (for example 1335 Hz, see figure 5.9), but in the model the eigenfrequency is not at this frequency, so no fair comparison would be possible.
Four results are made from the calculation of the model, one of the calculated frequency and three around this frequency. The reason for this is that the factor that is introduces is maybe not exactly 1.15. The complete results of the comparison can be seen in appendix G. Here only the results from the calculated shifted frequency will be shown.

The measurements are performed between 250 and 2500 Hz with steps of 250 Hz. All the measurements are performed with a different acceleration, so it is not possible to compare the results from 500 Hz with 1000 Hz and conclude something about the difference in sound pressure between those two. It is only possible to conclude something about the sound pressure level between the experiments and the model for each frequency separately.

In figure 5.10 the results of the model and the experiment are plotted for five frequencies. The pressure measured at the end of the tube is also plotted in this figure, but it must be mentioned that it is measured just outside the tube (about 5mm), so a different result from the model and the experiment is expected.

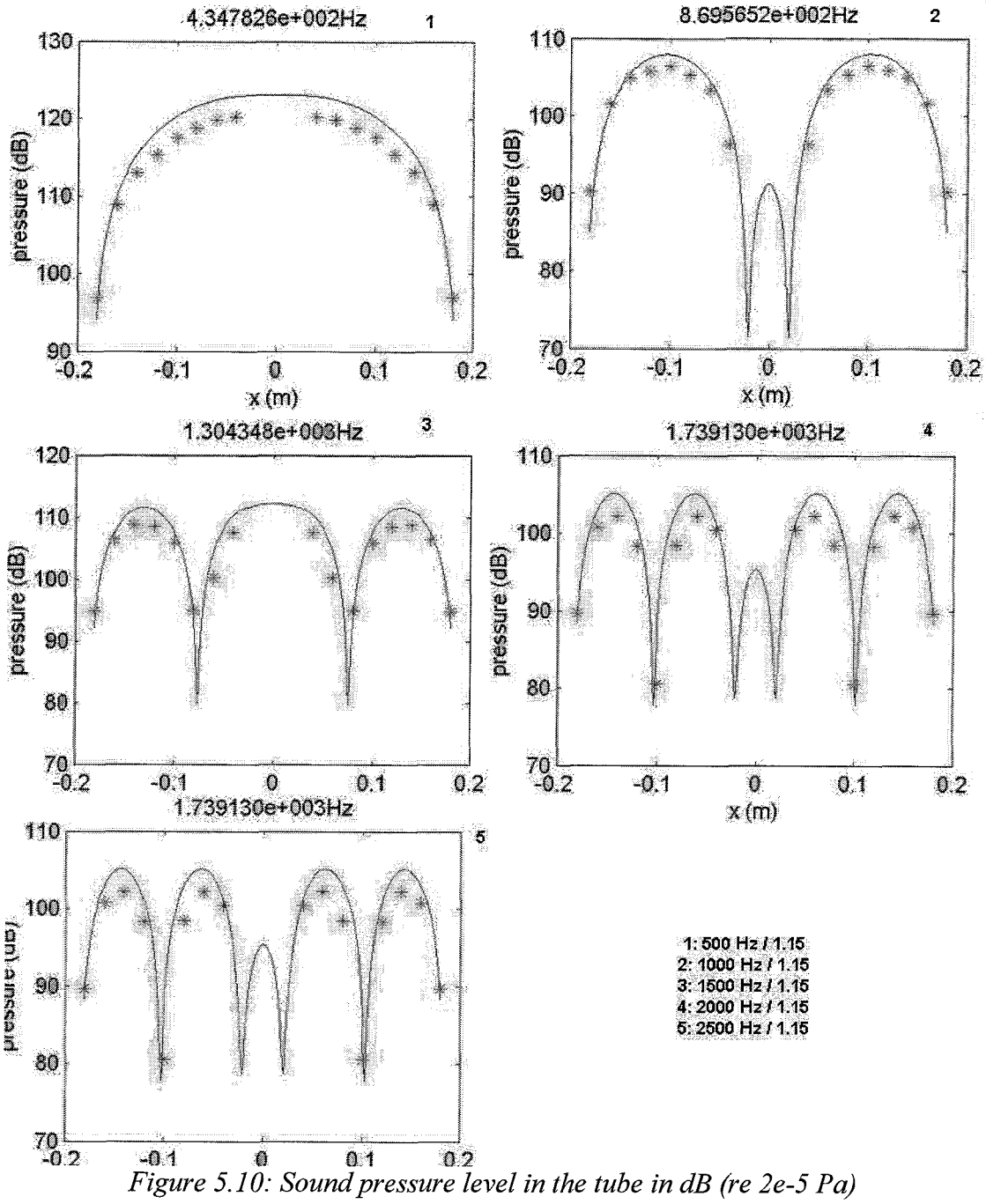

Figure 5.10: Sound pressure level in the tube in dB (re 2e-5 Pa)

The conclusion is that there is a good fit between the results. However it looks like the model overestimates the pressures a bit, which has various reasons. One can be that during the measurement the baffled end was not large enough to simulate a real baffled end. However it is hard to say how large this effect is so further measurements/calculations are needed. Another reason is that the input of the model is a bit too high. The simulation is performed at the average acceleration of the two accelerometers, but in reality the real average acceleration can be lower.

5.5.3: Conclusions of comparison between measurements and model

It can be concluded that the results from the experiments and the model are about the same. However the match between the model and the experiment becomes less evident if the frequency is high. This can have two reasons: First the measurements

can be wrong and second the reduced frequency (k) is already quite high (0.2). The main reason is that the measurements are not that good anymore at those high frequencies, because the patch is not vibrating everywhere with the same acceleration, so the model is not valid anymore.
But in general it can be concluded that it is a powerful tool for the tyre/road noise problem and then especially for the vibrating walls in tyre grooves.

5.6: Results model with tyre tread parameters

To simulate all the possible dimensions of a tyre profile tube is beyond the goals of this report. The calculations are performed with the next dimensions for the tube:
Table 4

	Length part 1	*Length part 2*	*Length part 3*	*Width*	*Heigth*
Tube	20 mm	20 mm	20 and 40 mm	10 mm	1, 3 and 5 mm

This results in two tubes where for each tube the force on the patch and the far field noise will be calculated. They all will be normalized with the acceleration in m/s^2.
The far field noise figure consists of the far field noise at 1 meter and with two angles of 0 rad. Not only the far field noise of the tube is plotted in the figures, but there is also a line plotted that is called "free", which is the far field noise that would be generated by the patch of 20 x 10 mm if it would be vibrating in a wall.

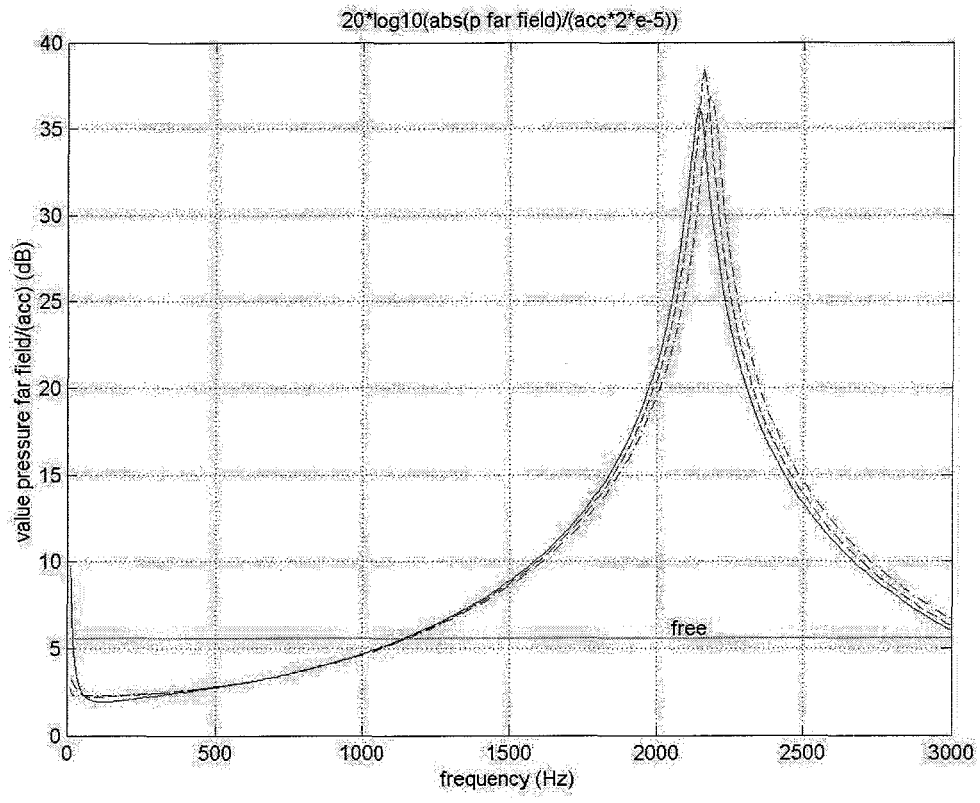

Figure 5.11: Far field sound 202020 tube (re 2e-5 Pa) (-=1 mm,--=2.5 mm and -.=5 mm)

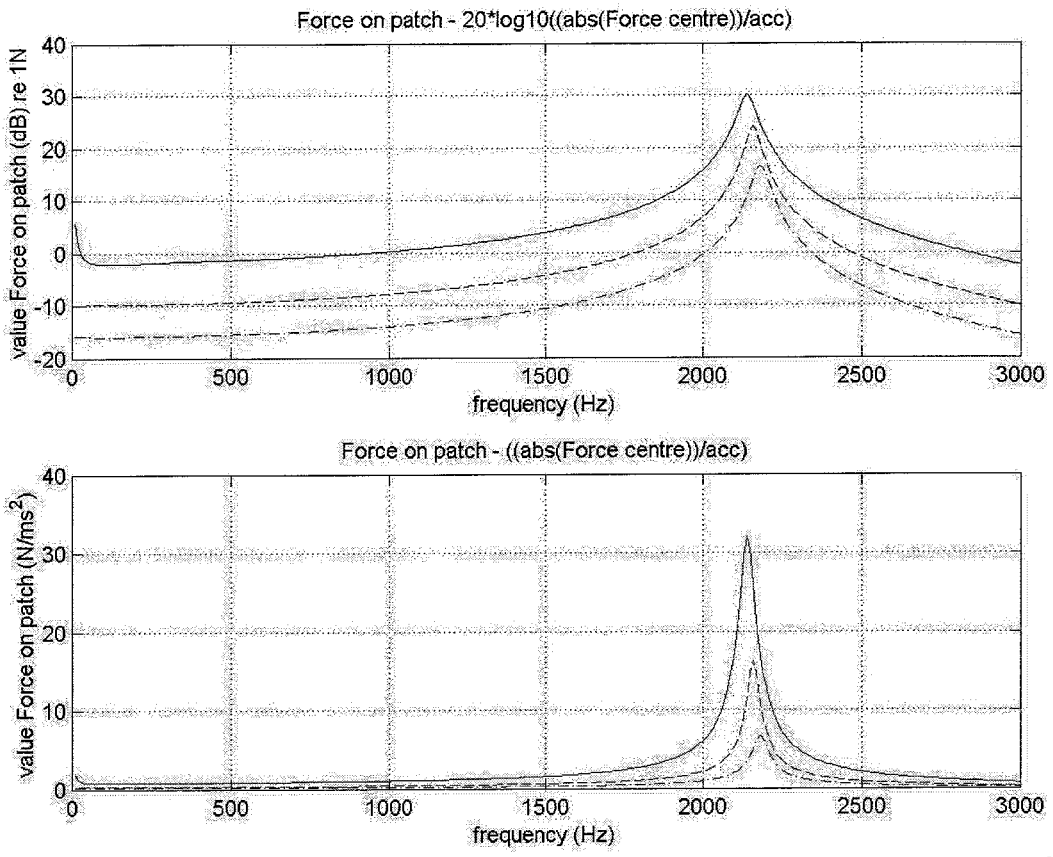

Figure 5.12: Force on the patch 202020 tube (re 2e-5 Pa) (-=1 mm,--=2.5 mm and -. =5 mm)

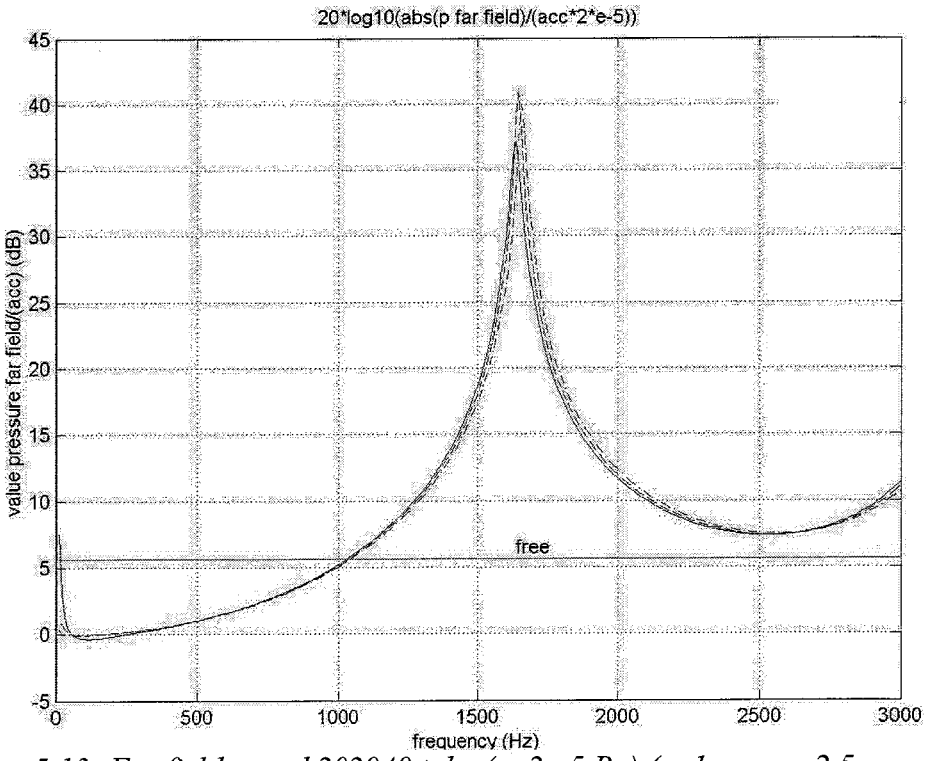

Figure 5.13: Far field sound 202040 tube (re 2e-5 Pa) (-=1 mm,--=2.5 mm and -. =5 mm)

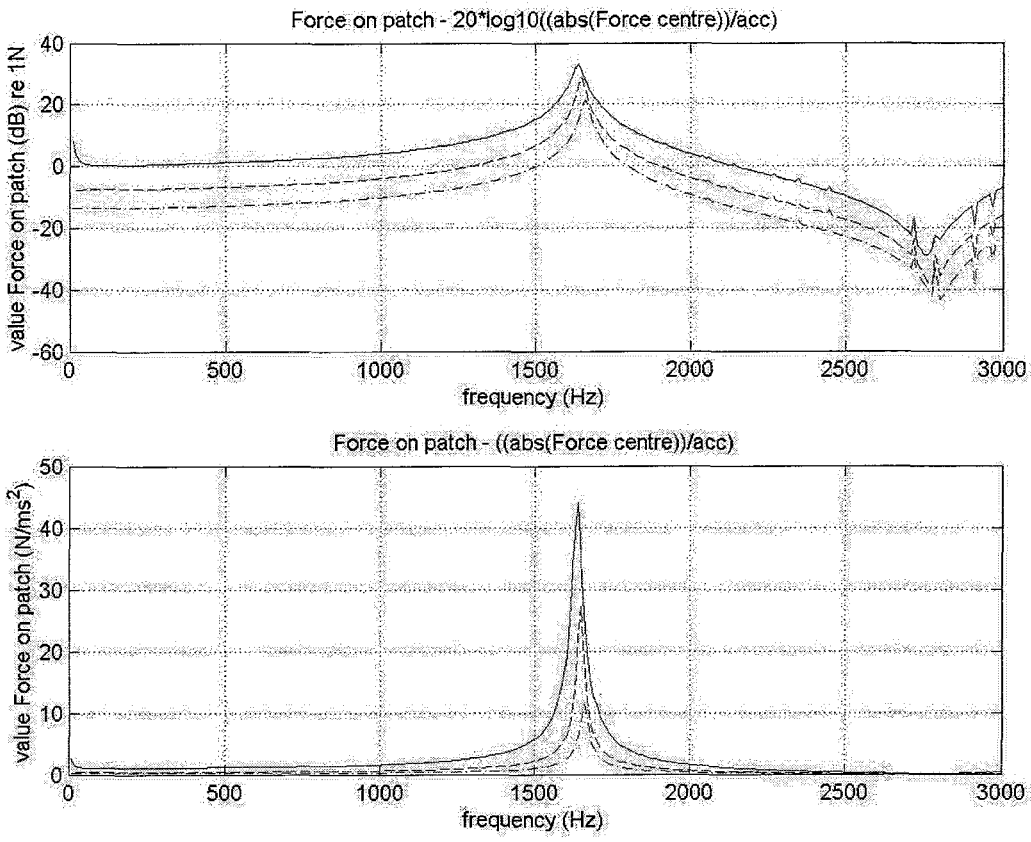

Figure 5.14: Force on the patch 202040 tube (re 2e-5 Pa) (-=1 mm,--=2.5 mm and -. =5 mm)

5.7: Conclusions regarding the model

The first conclusion from the simulations is that the force on the patch increases if the height of the tube is decreased. Also the eigenfrequency of the tube decreases if the height of the tube is decreased, but this effect is small.
At this moment it is not possible to say what happens with the eigenfrequency of the patch, because the calculation of this eigenfrequency is not implemented in the model. It is hard to draw conclusions about the far field noise, because it depends on the configuration of the tube, but there is an amplification at the resonance frequencies of the tube. Also the level of the far field sound is not directly related to the height of the tube. The reason for this is that the pressure and velocity at the end of the tube can be larger if the gap size gets smaller, but also the area of the tube gets smaller. Those two effects vanish against each other.

Chapter 6: Translation to tyre/road noise problem

In this chapter the two models will be used to predict the effect of the air in small gaps around the tyre for different mechanisms, which are discussed in chapter 2. Data of calculations performed with a tyre with grooves in circumferential direction on an ISO-road is available. A point on the tyre is taken and it is followed how it enters the contact patch and leaves it again. The distance between the road and the point is calculated and from this the distance, the velocity and acceleration are determined. The values of the frequencies and the values of the acceleration levels, which are the input parameters for the model, are calculated from this data.

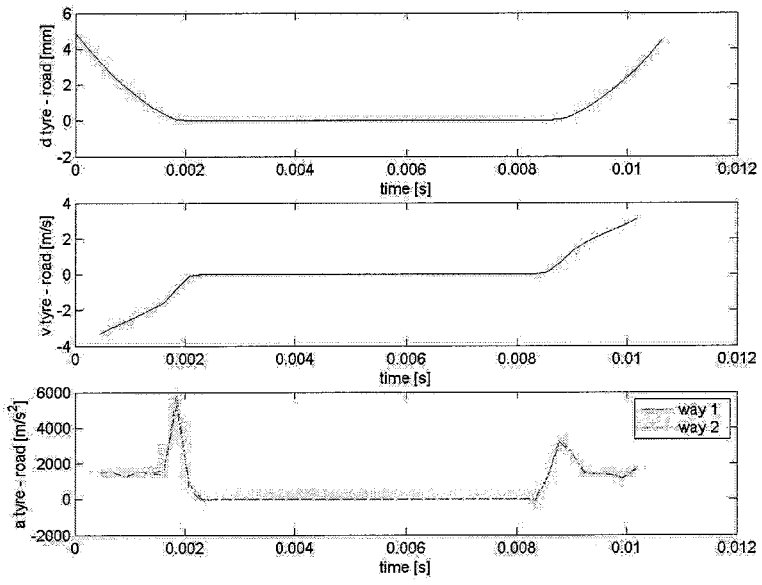

Figure 6.1: distance, velocity and acceleration against time of a point on the tyre (60 km/h)

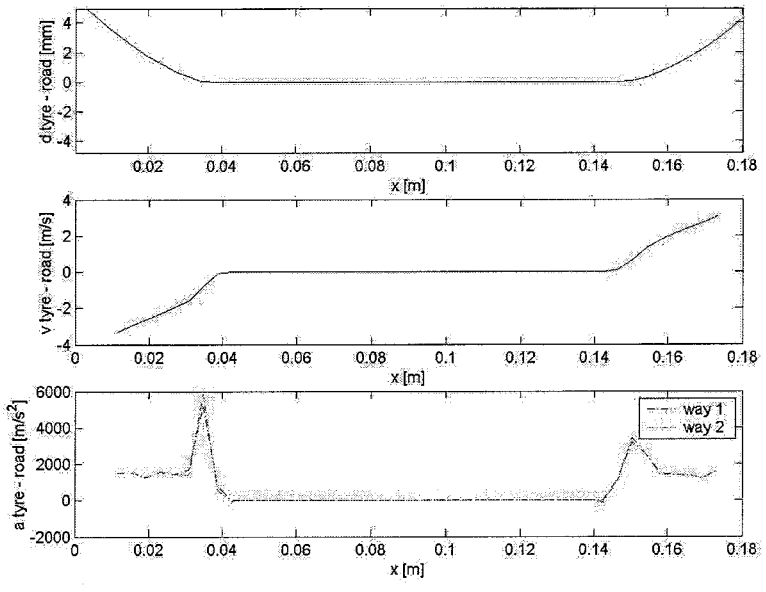

Figure 6.2: distance, velocity and acceleration against traveled distance of a point on the tyre (60 km/h)

6.1: Adhesion (stick-snap)/running deflection

These are effects that cause vibrations just in front and after the contact patch. The paragraph will be divided in two parts. In the first part vibrating tyre treads and the corresponding forces will be discussed and in the second part the vibrations due to the tyre movement and the corresponding forces will be discussed.

6.1.1: Vibrations of tread block

In figure 6.1 the data is plotted versus the time, in figure 6.2 the data is plotted versus the traveled distance. The region between 0 and 4 mm is interesting, because above the 4-5 mm the pressure/force that is build up is much smaller than between 0-4mm. The interesting frequency is 3000 Hz, because this is the eigenfrequency of the mode related to the adhesion mechanism of a tyre tread block [8]. From figure 6.1 it can be conclude that the point travels from 0 to 4 mm distance in 0.0018 s. Five cycles of a vibration of 3000 Hz fit into this period. From figure 6.2 can be concluded that the distance the point travels in this time is about 3 cm. Using this distance, a tyre tread of 2 cm fits once and a tread block of 1 cm fits twice in this region.

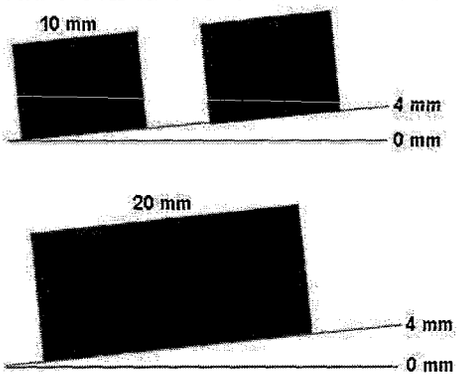

Figure 6.3 Tread blocks in the "vibrating" zone

Model A consists of a patch vibrating perpendicular to the ground, but the tread blocks in figure 6.3 are not fully perpendicular to the ground, but they will be modeled as perpendicular patches. In the first case in figure 6.3 there are 2 blocks vibrating; one at an average distance of 1 mm and one at an average distance of 3 mm. In the second case of figure 6.3 the system is translated in a patch vibrating 2 mm above the ground.
The calculations for a tyre tread of 10x10mm, at 2800-3200 Hz at 1 mm and 3 mm height with acceleration amplitude of 3000 m/s^2 are shown in figure 6.4. The value of 3000 m/s^2 is determined out of the calculated peak values at the trailing edge in figure 6.1.

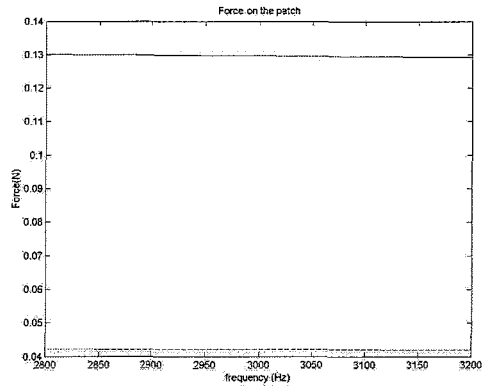

Figure 6.4: Force on a patch of 10x10mm with an acceleration amplitude of 3000 m/s^2 (solid:1mm, --:3mm)

For a typical tyre tread block the mass is around 3.63 10^{-4} kg [8], so the force becomes 3.63 10^{-4} kg*3000m/s^2=1.0890 N. The force delivered by the air onto the patch is around 0.12 N if the distance is 1 mm. The force delivered by the air onto the patch is around 0.045 N if the distance is 3 mm, so these forces do not have a significant influence on the vibration of the tyre tread blocks.
The calculations for a tyre tread of 20x20mm, at 2800-3200 Hz at 2 mm height with an acceleration of 3000 m/s^2 are shown in figure 6.5:

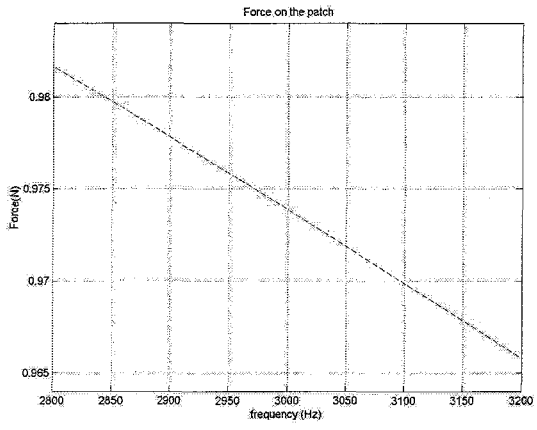

Figure 6.5: Force on a patch of 20x20mm with an acceleration amplitude of 3000 m/s^2 (distance is 2mm)

Again using the typical mass of a tyre tread block the force becomes 1.0890 N. The force delivered by the air onto the patch is around 1 N if the distance is 2 mm, so this force does have a significant influence on the vibration of the tyre tread block. It works against the vibration, because the force of the air is in opposite direction of the force due to the acceleration of the patch.

6.1.2: Tyre movement:

Here conclusions regarding a tyre tread approaching and leaving the contact patch due to tyre rotation will be drawn. A tread will travel in 0.0016 s from 1 to 5 mm (figure 6.1). This can be seen as a half period of a sinusoidal function, so it can be translated into a vibrating patch. These approximations result in the next parameters:

Table 5

	frequency	*amplitude*	*Length*	*Width*	*Heigth*
Patch	312.5 Hz (1/0.0032)	2 mm	10 and 20 mm	10 and 20 mm	3 mm

The calculation for a tyre tread of 10x10mm and 20x20mm, at 200-400 Hz at 3 mm distance with an amplitude of 2 mm is shown in figure 6.6:

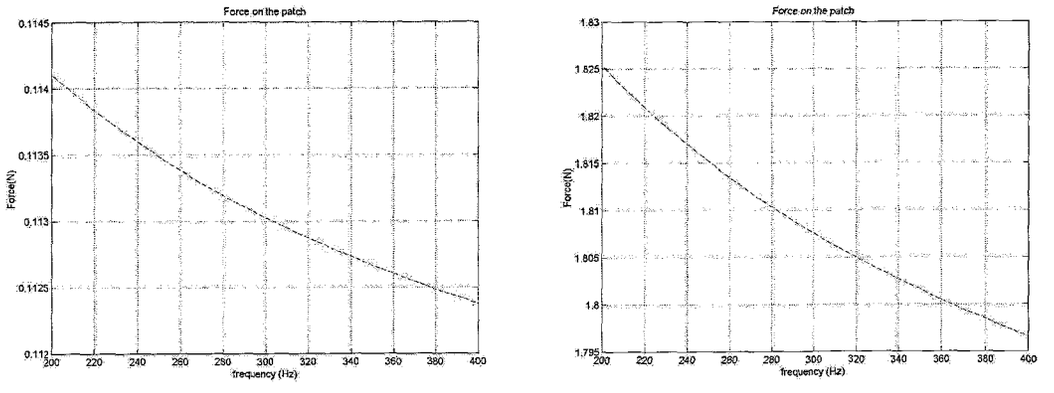

Figure 6.6: Force on a patch of 10x10mm (left) and 20x20mm (right) with an acceleration amplitude of 3000m/s^2 (distance is 3mm)

The force becomes 3.63 10^{-4} kg*7710m/s^2=2.8 N using the typical tyre tread mass [8] and the acceleration amplitude. The force delivered by the air onto the patch is around 0.12 N for the patch of 10x10 mm, so this force does not have a significant influence on the vibration of the tyre tread block. The force delivered by the air onto the patch of 20x20mm is around 1.8 N, so this force does have a significant influence on the vibration of the tyre tread block. On the trailing edge the pressure is build up, because tyre tread goes down, so the force will push the tread block further into the belt. On the trailing edge there is a pressure drop, because the tyre tread goes up. Due to the pressure drop the force will pull on the tyre tread and pull it out of the belt. It is now possible to see this force as an "impulse" force that pulls the system in the eigenfrequency-vibration.
This model is a large simplification of the reality, so it is difficult to say how valid the conclusions are in this case.

6.2: Stick-slip/airpumping/belt-vibration

Gagen [9] concludes that the density of the air can increase up to 10 % in cavities/ in the profile. This is something to remember when model B is used for tyre/road noise.
The vibration of a patch on the topside of a groove in the circumferential direction of the tyre will be simulated. Just after the tyre has left the contact patch the belt is vibrating. This can be seen in figure 6.1 and 6.2 as an acceleration-peak. The belt that is vibrating will be simulated as a patch in a tube that simulates the groove in circumferential direction. The tube that will be used in model B is constructed in the next way:
Table 6:

	Length part 1	*Length part 2*	*Length part 3*	*Width*	*Heigth*
Tube	10 mm	10 mm	100 mm	10 mm	3 mm

Part one simulates the part of the profile just after the contact patch.
Part two has the width of the acceleration peak in figure 6.2.

Part three is the length of the contact patch as can be seen in figure 6.2.

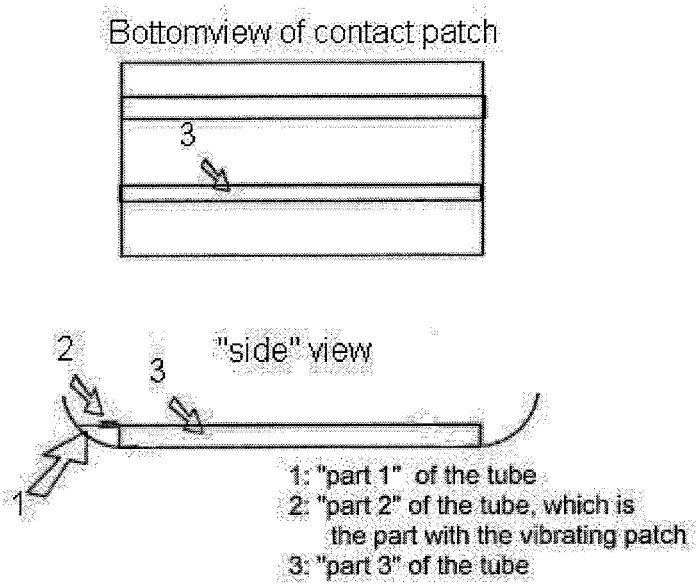

Figure 6.7: Tyre profile

The height will be set to 3 mm and the width to 10 mm, which are just standard parameters of a tyre groove. Adhesion does not have an effect in the tube, because the vibration of the patch is caused by a part of the tyre that is not in contact with the road. The frequency is 500Hz. This is a result of the next calculation:. The width of the peak is about 0.001 s. This is a half period of a sinusoidal function, so this results in a frequency of 500 Hz. For the acceleration 3000 m/s^2 can be taken according to figure 6.1 and 6.2. The results of the calculations for this tube, at 300-800 Hz at are shown in figure 6.8. This frequency range is chosen to get a total view of the forces around the 500 Hz.

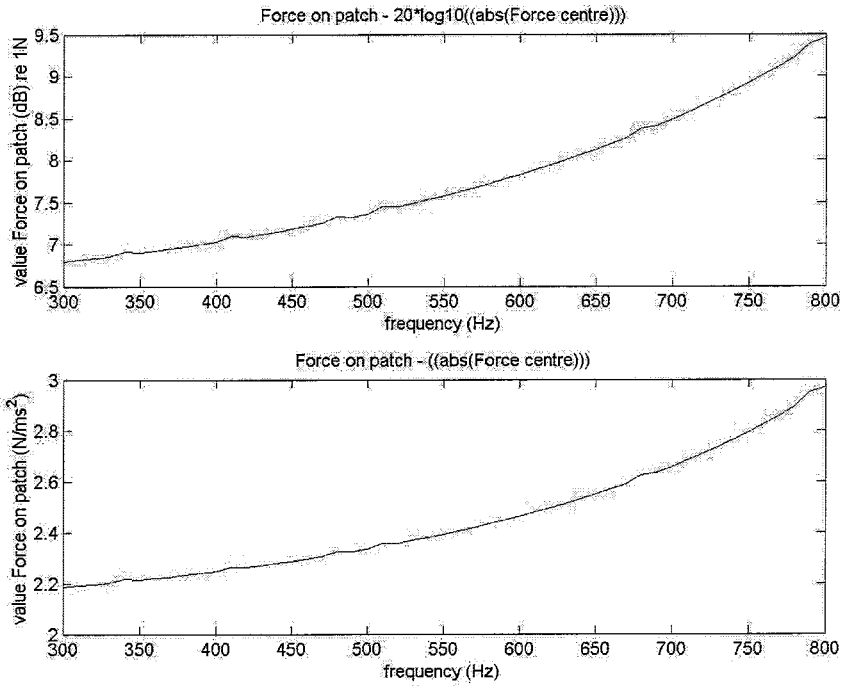

Figure 6.8: Force on the vibrating patch due to the air with an acceleration amplitude of 3000 m/s^2 .

The force in this case is 3.63 10^{-4} kg*3000m/s^2=1.0890 N using the typical tyre tread mass [8]. The force delivered by the air onto the patch is around 2.4 N, so this force has a significant influence on the vibration even if the mass of the patch is in reality a bit larger due to the fact that the patch is a part of the belt. The conclusion is that there is quite a large force due to the air working against the vibration of the belt.

6.3: Conclusions

In general it can be concluded that the air has an effect on the vibrations of the patch/tread block. However in "free" air, so not in a tube, the effect is only large on patches of reasonable size (20x20mm). However in a tube the effect is also large for smaller patches (10x10). The force that works on the patches works against the vibrations in most cases. Only in the case of the tread block in combination with the tyre movement it maybe will introduce vibrations. In reality the forces/vibrations of patches/tyre treads will be smaller than calculated with the model, because the model is a simplification of the reality and in reality the surface is not completely smooth as supposed here.

Chapter 7: Conclusion and recommendations

Conclusions:

The *objectives* of this project are to investigate to what extent the dynamic load of the surrounding air will influence the vibrations on a tyre during tyre/road interaction and to investigate to what extent the narrow geometry will influence the radiation from the contact patch.

Two models of patches vibrating in narrow geometries are used to study and estimate the air load and radiation of sound for some cases of the tyre/road interaction. The models are based on work done by Beltman's [1][2] and the main approximations in the calculations was done to the input data, with simplifications of the geometry, pressure and velocity boundary conditions, while the model is general and validated for several cases.

The effect of the air load, in a small gap between tyre and road, on the vibrations of the tyre is predicted using the narrow geometry models and data from Chalmers tyre model. A significant effect is predicted for a normal passenger car tyre around 60 km/h. The air load on the patches is of the same magnitude as the forces needed to create the calculated vibrations. At the trailing edge, when the tread block is leaving the contact patch, the air load will introduce vibrations in the block. It can be concluded that the calculations show that in reality the forces/vibrations of patches/tyre treads will be slightly different than calculated with the Chalmers tyre model, because the tyre model neglects the effect of the air load.

It looks like the far field sound / radiation does not change with the gap size, but changes with the vibration of the patch. This result comes from the model but it must be named that the model is not validated for the far field sound, because it was not possible to measure the far field sound of the experiment due to the surrounding noise from for example the shaker. However the expectation is that the far field sound equation is correct.

It is proven by this report that the low reduced frequency model is suitable to solve these type of problems, because it is also possible to make gaps very small and still be able to say something about the forces/eigenfrequency changes.

To summarize, the effect of the air load due to the narrow geometry may be significant. However, further investigations, especially on the input data, are needed to get more precise quantitative predictions.

The goals of this research are achieved, but there is still a lot that can be done to get more and better results so that the model for the tyre/road noise from the Chalmers University will be improved. Some of the things that can be done in the future will be discussed now.

Recommendation/Future work

It is necessary to do a further research to the problem with the B function described in chapter 5. At this moment (March 2004) the problem is submitted to the University Twente in Holland where the low reduced frequency model is developed, but no results are achieved yet.

It is important to validate the far field sound equation to make sure that the conclusions regarding the effect of the air on the far field sound is correct.

It can be interesting to have more vibrating patches inside a tube. For example a longitudinal groove with 2 patches; one almost in the beginning simulating the leading edge and one almost at the end simulating the trailing edge. This is possible by expanding the matrices of the linear system that describes the tube.
Another recommendation is to see to what extend the effects found here are also present in a real life situation with varying track surface. It could also be interesting to research the effects at higher speeds than 60 km/h. Lower speeds are not that interesting, because the lower the speed the less relevant the tyre/road noise is for the total noise of the car.
It is interesting to see to what extend the FEM element, based on the low reduced frequency model, can be used for these type of problems.
Finally a time domain formulation of the low reduced frequency model can be interesting, because with this it is possible to really simulate a tyre tread approaching the track surface.

References

[1] W.M. Beltman. Viscothermal wave propagation including acousto-elastic interaction ISBN 90-3651217-4 (1998)

[2] W.M. Beltman, P.J.M. van der Hoogt, R.M.E.J. AIR LOADS ON A RIGID PLATE OSCILLATING NORMAL TO A FIXED SURFACE, Journal of Sound and Vibration (1997) 206(2), 217–241

[3] Ulf Sandberg en Jerzy A. Ejsmont. Tyre/Road noise-Reference Book (2002) INFORMEX, Harg, SE-59040 Kisa, Sweden

[4] Wolfgang Kropp. "A mathematical model of Tyre Noise Generation, International Journal of Vehicle Design (IJVD)",Vol 6, Nr 1-4, (1999)

[5] Tijdeman, H., On the propagation of sound waves in cylindrical tubes, Journal of Sound and Vibration. 1975, 39(1), 1-33.

[6] P.M. Morse and K.U. Ingard. Theoretical Acoustics. *Princeton University Press*, Princeton, 1st edition, 1968.

[7] R.M. Aerts and A.J.E.M. Janssen. Approximation of the Struve function H1 occurring in impedance calculations, J. Acoustic Soc. Am 113(5) May 2003

[8] Krister Larsson. Modelling of Dynamic Contact – Exemplified on the tyre/road interaction [2002] ISBN 91-7291-146-8

[9] M.J. Gagen
1: Supersonic expelled jets from squeezed fluid singularities,*epartment of Physics, University of Queensland, Qld 4072, Australia (*June 8, 2000)
2: Novel acoustic sources from squeezed cavities in car tires
(J. Acoust. Soc. Am. 106(2) 794-801 [1999]

[10] http://ceta.mit.edu/comp_spec_func/ [11 december 2003]
A Matlab file for an approximation of the Struve function.

[11] Frédéfic Wullens. Towards an Optimization of tyre tyre/road parameters for noise reduction. [2002] ISSN 0283-832X F02-01

[12] Patrik Andersson. High frequency tyre Vibrations. [2002] ISSN 0283-832X F02-04

[13] Stanners D. and Bourdeau P. (eds.). 1995. Europe's Environment: The Dobris Assessment. *European Environment Agency. pp xxiv + 676. ISBN 92 826 5409 5.*

List of symbols

Symbol	Quantity	Unit
A	The function describing velocity and temperature profiles	-
A^{cd}	Cross-sectional area	-
a	Length factor	-
a,b	Dimensions opening tube for the end-impedance calculation	m
A1, A2, B1, B2, C1, C2, p_{x1},p_{x2}	Model parameters problem 2	-
B	The function accounting for viscous or thermal effects	-
C	The function describing the temperature profile	-
c_0	Undisturbed speed of sound	m/s
C_v	Specific heat at constant volume	J/kgK
C_p	Specific heat at constant pressure	J/kgK
D	The function describing the temperature profile	-
F_m	Driving force	N
F_{patch}/F_{gap}	Force due to the pressure distribution in the gap	N
$g_{m,e}(t)$	Greens function	m/N
h	Dimensionless amplitude patch	-
i	Imaginary unit	-
J_1,J_0	Bessel functions	-
k	- Reduced frequency - Angular frequency divided by the speed of sound - Spring stiffness	- rad/s N/m
k_x	Wave number in x direction	-
L	Dimensionless amplitude patch in tube	-
l_x,l_y,l_z,h_0,L_0	Dimensions tube and patch	m
m	mass	kg
M_1,M_0	Struve functions	-
$n(s\sigma)$	The polytropic constant	-
p	Dimensionless pressure amplitude	-
p_0	Mean pressure	N/m^2
$\overline{p}$	Pressure	N/m^2
Q_1,Q_2	Parameters of the functions A and B for problem 2	-
r	Reflection factor	-
$\Re$	The function which states how and which part of the construction vibrates	-
R_0	Gas constant	J/kgK
S1, S2	Area of tube cross-section	-
s	Shear wave number	-
t	Time	s

Symbol	Quantity	Unit
T	Dimensionless temperature amplitude	-
T_0	Mean temperature	K
$\overline{T}$	Temperature	K
$\overline{v}$	Velocity vector	m/s
v^{pd}	Velocity in the propagation coordinate(s) direction	-
v	Dimensioless velocity	-
x^{pd}	Coordinate(s) in the propagation direction	-
x^{cd}	Coordinate(s of the cross section	-
Z	End-impedance	$N/m^2/m/s$
Z_r	Radiation impedance	N/m/s
Γ	The propagation constant	-
γ	Ratio of specific heats	-
η	Bulk viscosity	Ns/m^2
ϑ	The vertical angle between the normal line through the piston and the position of the receiver	rad
ξ_e	Displacement at point e	m
λ	Thermal conductivity	W/mK
μ	Dynamic viscosity	Ns/m^2
$\overline{\rho}$	Density	kg/m^3
ρ_0	Mean density	kg/m^3
ρ	Dimensionless density amplitude	-
φ	The horizontal angle between the normal line through the piston and the position of the receiver	rad
σ	Square root of the Prandtl number	-
ω	Angular frequency	Rad/s
$\overline{\nabla}$	Gradient operator	-
∇^{pd}	Gradient operator in propagation coordinates	-
$\overline{\Delta}$	Laplace operator	-
Δ^{cd}	Laplace gradient in the cross-sectional coordinates	-

Appendix A: Validation of model A

In this appendix the validation of model A will be shown.
One change to the formulas found in [1] is made; the formula for $F_{gap,}$ formula 4.8 [1] is changed, because the k_x^4 must be k_x^2. This can be concluded from formula 4.12 [1] and also from formula B24 (Beltman 1997 [2]).

A.1: Experiment

A stiff plate (solar panel) of 0.98m x 0.98m is fixed with 8 springs just above a flat panel. It is driven at the center at relative low frequencies (1-10Hz). The pressure is measured at three different points (center, halfway and at the edge).
The setup was mainly used to measure the shift in eigenfrequency and the pressure distribution in the gap.

The following properties of interest are used in the model [1]:

$m = 2.540kg$ $\quad \rho_0 = 1.2kg/m^3$
$l_x = 0.49m$ $\quad c_0 = 343m/s$
$l_y = 0.49m$ $\quad \lambda = 25.6 \cdot 10^{-3} W/mK$
$R_0 = 287J/kgK$ $\quad \mu = 18.2 \cdot 10^{-6} Ns/m^2$
$C_p = 1004J/kgK$ $\quad \kappa = 1186N/m$
$C_v = 716J/kgK$ $\quad T_0 = 290K$

A.2: Eigenfrequenties

The results achieved with the Matlab file written by Vissers (2003) are shown in fig A.1. Also the results from the experiment performed by Beltman are shown in this figure. The exact results can be found in [1].

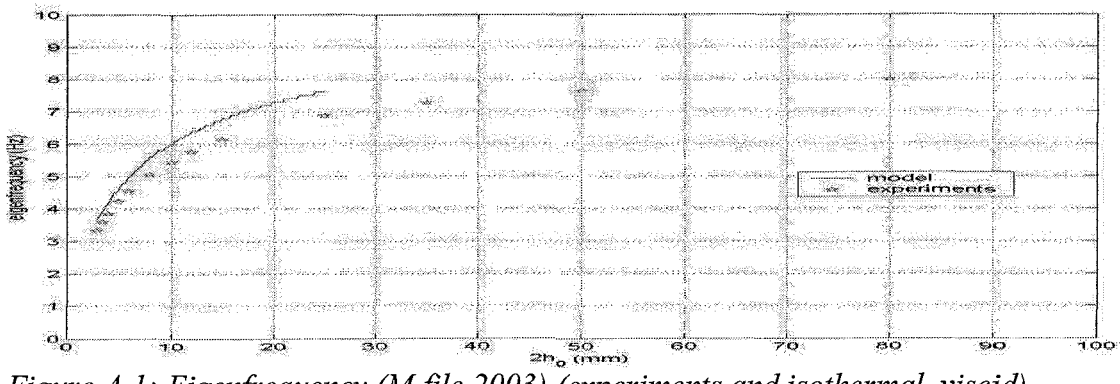

Figure A.1: Eigenfrequency (M-file 2003) (experiments and isothermal, viscid)

As can be seen the same result is shown as in figure 4.8 [1].
The eigenfrequencies of the adiabatic, inviscid system are plotted in one figure (figure A.2)

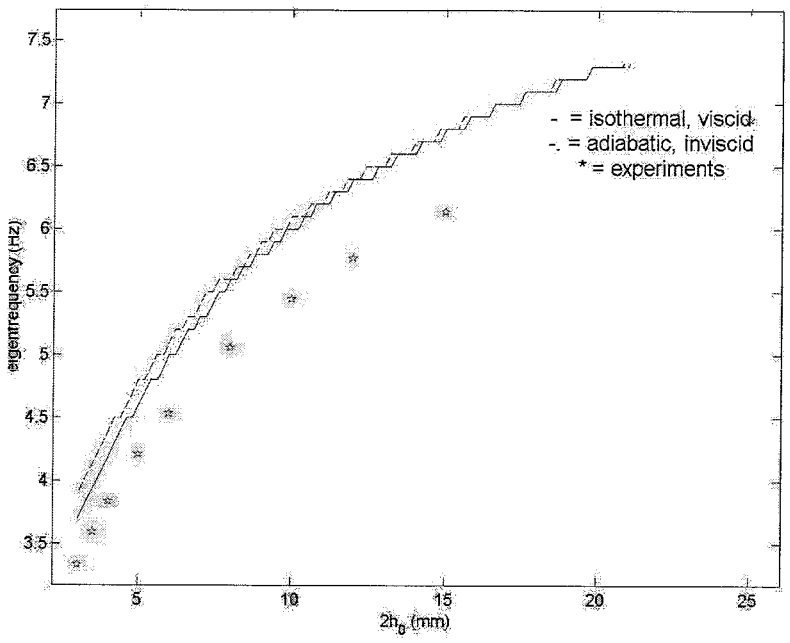

Figure A.2: Eigenfrequency (M-file 2003) (isothermal, viscid and adiabatic inviscid)

From figure A.2 can be concluded that the isothermal, viscid system is a better approximation if the gap becomes smaller. For larger gaps there is almost no difference.

A.3: Pressure

In the first figure the pressure at the *center of the plate* (p_1) is shown for the experiments, the low reduced frequency model, the inviscid and adiabatic low reduced frequency model (Γ=i and $n(s\sigma)=\gamma$). At the last figure the pressure *halfway the plate* (p_2) is shown. The real pressure is divided by h_0h, which is the amplitude of the plate. The dividing is done to give a more general impression of the pressure. The pressure in the layer is frequency dependent so that is the reason why the pressure was measured at the eigenfrequency for each gap. The figure can now be used for all amplitudes, because the value in the figure just has to be multiplied by the amplitude and than the pressure for that specific amplitude can be determined.

The results achieved with the Matlab file are shown in figure A.3 – A.6:

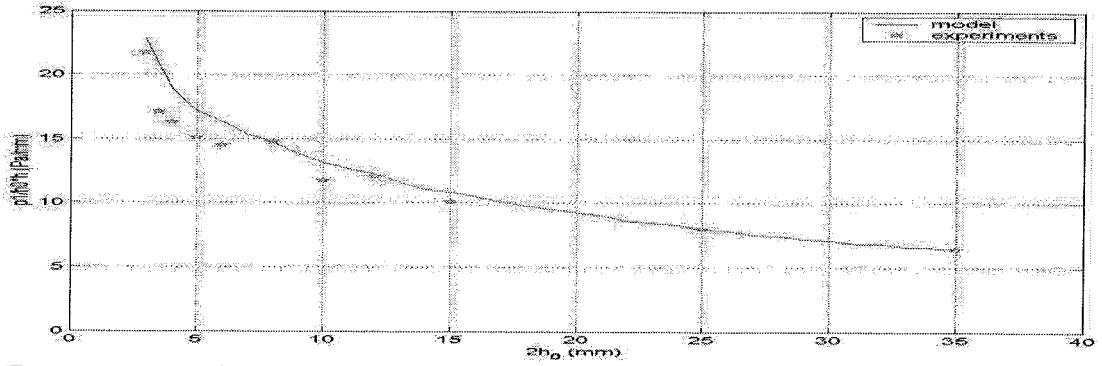

Figure A.3: Scaled pressure p1 for the experiments and the low reduced frequency model.

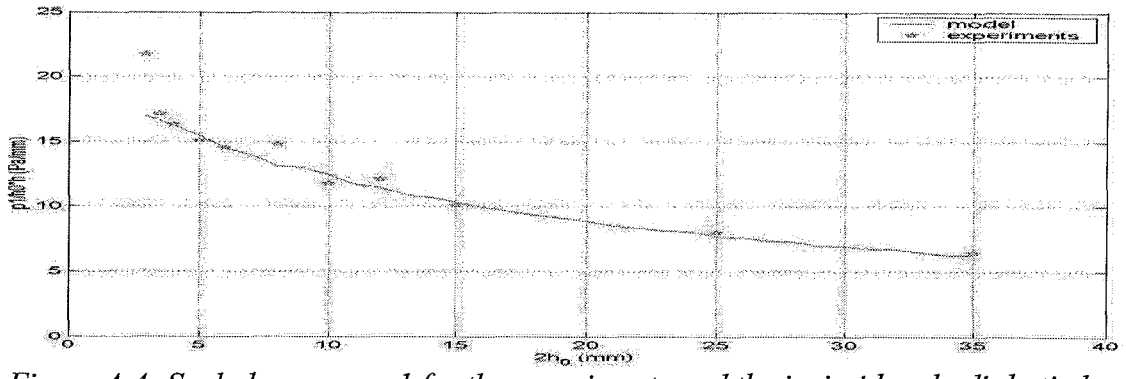

Figure A.4: Scaled pressure p1 for the experiments and the inviscid and adiabatic low reduced low reduced frequency model.

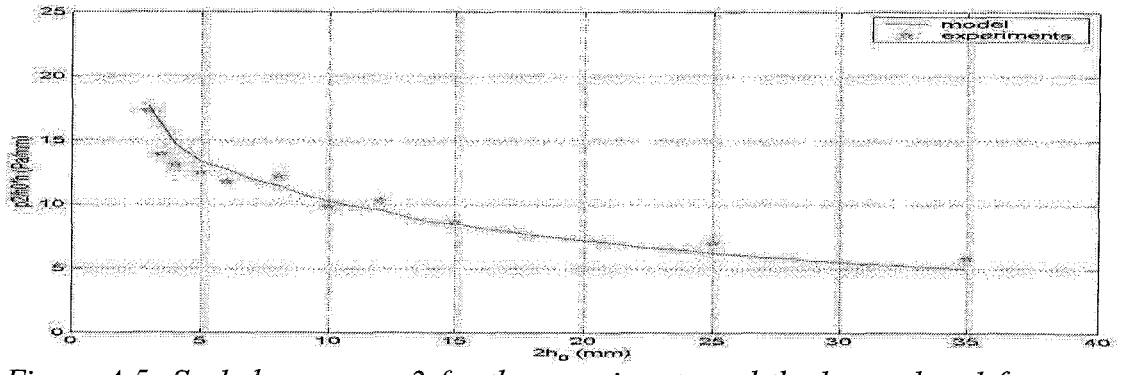

Figure A.5: Scaled pressure p2 for the experiments and the low reduced frequency model with isothermal walls.

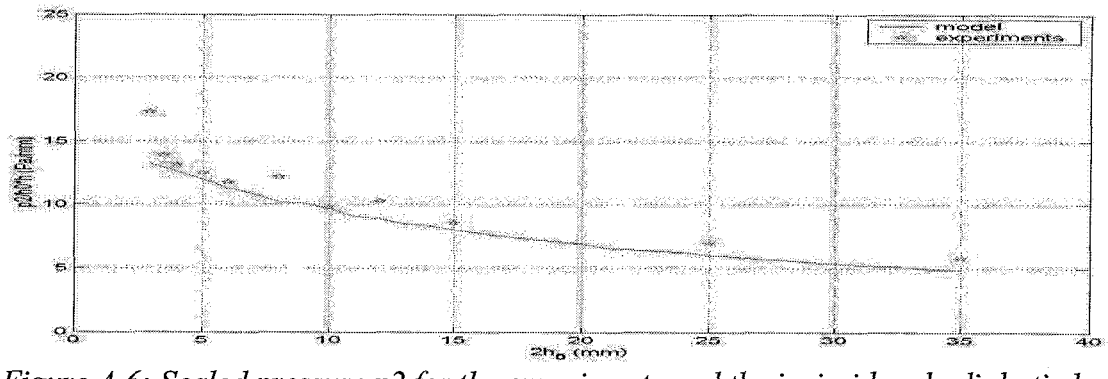

Figure A.6: Scaled pressure p2 for the experiments and the inviscid and adiabatic low reduced low reduced frequency model.

Again the results from the matlab file match with the results from [1] so it can be concluded that the Matlab model is valid. Now it is important to look if the low reduced frequency model can be used to study tyre tread blocks.

Appendix B: Low reduced frequency model for a plate

Deviation of the low reduced frequency for a plate vibrating just above the ground.

Basic:

$$\Delta^{pd} P(x^{pd}) - k^2 \Gamma^2 p(x^{pd}) = -ikn(s\sigma)\Gamma^2 \Re$$

$$\Gamma = \sqrt{\frac{\gamma}{n(s\sigma)B(s)}}$$

$$n(s\sigma) = \left[1 + \left[\frac{\gamma - 1}{\gamma}\right] D(s\sigma)\right]^{-1}$$

$$B(s) = \frac{1}{A^{cd}} \int_{A^{cd}} A(s, x^{cd}) dA^{cd}$$

$$D(s\sigma) = \frac{1}{A^{cd}} \int_{A^{cd}} C(s\sigma, x^{cd}) dA^{cd}$$

$$\Re = \frac{1}{A^{cd}} \int_{\delta A^{cd}} v \bullet e_n d\delta A^{cd}$$

Parameters for a rectangular plate [[1] appendix B]:

$$l = h_0 \qquad x = (x, y, z\ ) \qquad a = \frac{l_y}{l_x}$$

$$x = \frac{\omega \bar{x}}{c_0} \qquad y = \frac{\omega \bar{y}}{c_0} \qquad z = \frac{\bar{z}}{h_0}$$

$$\nabla = e_x k \frac{\partial}{\partial x} + e_y k \frac{\partial}{\partial y} + e_z \frac{\partial}{\partial z}$$

$$\Delta = k^2 \frac{\partial^2}{\partial x^2} + k^2 \frac{\partial^2}{\partial y^2}_{z} + \frac{\partial^2}{\partial z^2}$$

$$x^{cd} = (z) \qquad x^{cd} = (x, y)$$

$$\nabla^{cd} = e_z \frac{\partial}{\partial z} \qquad \nabla^{pd} = e_x k \frac{\partial}{\partial x} + e_y k \frac{\partial}{\partial y}$$

$$\Delta^{cd} = \frac{\partial^2}{\partial z^2} \qquad \Delta^{pd} = k^2 \frac{\partial^2}{\partial x^2} + k^2 \frac{\partial^2}{\partial y^2}$$

$$A = \frac{\cosh(sz\sqrt{i})}{\cosh(s\sqrt{i})} - 1$$

$$B = \frac{\tanh(s\sqrt{i})}{(s\sqrt{i})} - 1$$

$$\Re = \frac{1}{2}\left[v_z(x,y,1) - v_z(x,y,-1)\right]$$

Also given:

$$\bar{v} = c_o v e^{i\omega t}$$

$$\bar{h} = h_o(2 + he^{i\omega t})$$

$v_z(x,y,-1)=0$, because the lowest plate is not moving

$v_z(x,y,1)= ?$

$$\bar{v}_z = c_o v_z e^{i\omega t}$$

$$\bar{v}_z = \dot{\bar{h}}$$

$$\dot{\bar{h}} = h_o hi\omega e^{i\omega t}$$

$$k = \frac{h_o \omega}{c_o}$$

These last 2 combined give:

$$\dot{\bar{h}} = kc_o hi\omega e^{i\omega t}$$

Because $\bar{v}_z = \dot{\bar{h}}$

$v_z=khi$

so $\Re = \frac{1}{2} khi$

This all combined gives:

$$\frac{\partial^2 p}{\partial x^2} + \frac{\partial^2 p}{\partial y^2} - \Gamma^2 p = n(s\sigma)\Gamma^2 \frac{1}{2} h$$

$$B(s) = \frac{\tanh(s\sqrt{i})}{s\sqrt{i}} - 1$$

$$n(s\sigma) = \left[1 + \left[\frac{\gamma - 1}{\gamma}\right] D(s\sigma)\right]^{-1}$$

Isothermal walls: $D(s\sigma)=B(s\sigma)$

Adiabatic walls: $D(s\sigma)=-1$

Appendix C: Low reduced frequency model for a patch in a tube

Deviation of the low reduced frequency for a patch vibrating in a tube

Basic:

$$\Delta^{pd} P(x^{pd}) - k^2 \Gamma^2 p(x^{pd}) = -ikn(s\sigma)\Gamma^2 \Re$$

$$\Gamma = \sqrt{\frac{\gamma}{n(s\sigma)B(s)}}$$

$$n(s\sigma) = \left[1 + \left[\frac{\gamma - 1}{\gamma}\right] D(s\sigma)\right]^{-1}$$

$$B(s) = \frac{1}{A^{cd}} \int_{A^{cd}} A(s, x^{cd}) dA^{cd}$$

$$D(s\sigma) = \frac{1}{A^{cd}} \int_{A^{cd}} C(s\sigma, x^{cd}) dA^{cd}$$

$$\Re = \frac{1}{A^{cd}} \int_{\delta A^{cd}} v \bullet e_n d\delta A^{cd}$$

Parameters for a tube plate (appendix B in [1]):

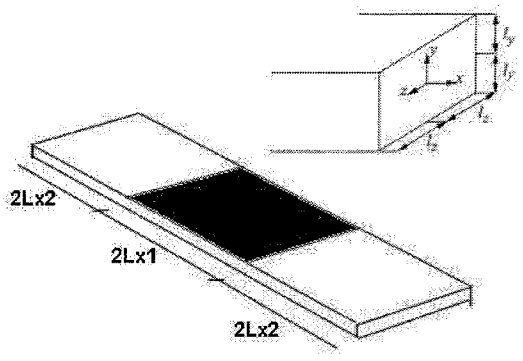

$$l = l_y \qquad x = (x, y, z\ ) \qquad a = \frac{l_z}{l_y}$$

$$x = \frac{\omega \bar{x}}{c_0} \qquad y = \frac{\bar{y}}{l_y} \qquad z = \frac{\bar{z}}{l_y}$$

$$\nabla = e_x k \frac{\partial}{\partial x} + e_y \frac{\partial}{\partial y} + e_z \frac{\partial}{\partial z}$$

$$\Delta = k^2 \frac{\partial^2}{\partial x^2} + \frac{\partial^2}{\partial y^2}_z + \frac{\partial^2}{\partial z^2}$$

$$x^{cd} = (y, z) \qquad x^{cd} = (x)$$

$$\nabla^{cd} = e_y \frac{\partial}{\partial y} + e_z \frac{\partial}{\partial z} \qquad \nabla^{pd} = e_x k \frac{\partial}{\partial x}$$

$$\Delta^{cd} = \frac{\partial^2}{\partial y^2} + \frac{\partial^2}{\partial z^2} \qquad \Delta^{pd} = k^2 \frac{\partial^2}{\partial x^2}$$

$$A = Q_1 \sum_{q=1,3...}^{\infty} \frac{-1^{\frac{q-1}{2}}}{qQ_2^2}\left[\frac{\cosh(Q_2 z)}{\cosh(Q_2)} - 1\right]\cos\left(\frac{q\pi y}{2}\right)$$

$$Q_1 = \frac{ia^2 s^2 4}{\pi}; Q_2 = a\sqrt{\left(\frac{q\pi}{2}\right)^2 + is^2}$$

$$B = Q_1 \sum_{q=1,3...}^{\infty} \frac{-1^{\frac{q-1}{2}}}{q^2 Q_2^2}\left[\frac{\tanh h(aQ_2)}{aQ_2} - 1\right]$$

$$Q_1 = \frac{ia^2 s^2 8}{\pi^2}; Q_2 = a\sqrt{\left(\frac{q\pi}{2}\right)^2 + is^2}$$

$$\Re = \frac{1}{4}\int_{z=-1}^{1}[v_y(x,1,z) - v_y(x,-1,z)]dz + \frac{1}{4}\frac{1}{a}\int_{y=-1}^{1}[v_z(x,y,1) - v_z(x,y,-1)]dy$$

Also given:

$\bar{v} = c_o v e^{i\omega t}$

$\bar{L} = L_o(2 + Le^{i\omega t})$

$v_z(x,y,-1)=0$ and $v_z(x,y,1)= 0$ because the sides are not moving.

$v_y(x,-1,z)= 0$, because the bottom is not moving.

$v_y(x,1,z)=$ not known yet if the top plate is moving.(If this is not the case than $v_y(x,1,z)=0$ and so $\Re = 0$)

$\bar{v}_y = c_o v_y e^{i\omega t}$

$\bar{v}_y = \dot{\bar{L}}$

$\dot{\bar{L}} = L_o Li\omega e^{i\omega t}$

$k = \frac{L_o \omega}{c_o}$

These last 2 combined give:

$\dot{\bar{L}} = kc_o Li\omega e^{i\omega t}$

Because $\bar{v}_z = \dot{\bar{L}}$

v_y=kLi

so $\Re = \frac{1}{2}kLi$

This all combined gives:

$$\frac{\partial^2 p}{\partial x^2} - \Gamma^2 p = n(s\sigma)\Gamma^2 \frac{1}{2}L$$

$$n(s\sigma) = \left[1 + \left[\frac{\gamma - 1}{\gamma}\right]D(s\sigma)\right]^{-1}$$

Isothermal walls: D(sσ)=B(sσ)

Adiabatic walls: D(sσ)=-1

(In this report only isothermal walls are used for the calculations)

Velocity
Defined in [1] as:

$$v^{pd}(s, x^{pd}, x^{cd}) = \frac{-i}{k\gamma} A(s, x^{cd}) \nabla^{pd} p(x^{cd})$$

$$\nabla^{pd} = e_x k \frac{\partial}{\partial x}$$

Appendix D: Analytic solution

In this appendix an analytic solution for 1 "simple" case can be found. It is for the case that the pressure at both ends is zero.

3 basic equations and 8 boundary conditions:

$$p_1 = -A_1 e^{-\Gamma x} + A_2 e^{\Gamma x}$$

$$p_2 = -B_1 e^{-\Gamma x} + B_2 e^{\Gamma x} - \frac{1}{2} n(s\sigma) L$$

$$p_3 = -C_1 e^{-\Gamma x} + C_2 e^{\Gamma x}$$

$$1: p_1(-k_{x1}) = 0$$

$$2: p_1(k_{x1}) = p_{x1}$$

$$3: p_2(-k_{x2}) = p_{x1}$$

$$4: p_2(k_{x2}) = p_{x2}$$

$$5: p_3(-k_{x3}) = p_{x2}$$

$$6: p_3(k_{x3}) = 0$$

$$7: \left.\frac{\partial p_1}{\partial x}\right|_{k_{x1}} = \left.\frac{\partial p_2}{\partial x}\right|_{-k_{x2}} : S1 \cdot v1 = S2 \cdot v2$$

$$8: \left.\frac{\partial p_2}{\partial x}\right|_{k_{x2}} = \left.\frac{\partial p_3}{\partial x}\right|_{-k_{x3}} : S2 \cdot v2 = S3 \cdot v3$$

It is not enough to just say that the pressures should be the same, because there also should be a smooth overlap from pressure 1 to pressure 2. That's why the conservation of mass is used.

1 and 2:
x=-k_{x1}:

$$p_1 = -\frac{A}{e^{\Gamma k_{x1}}} e^{-\Gamma x} + \frac{A}{e^{-\Gamma k_{x1}}} e^{\Gamma x}$$: So condition 1 is ok.

x=k_{x1}:
Insert k_{x1} in the formula that's just found:

$$p_{x1} = -A(e^{-\Gamma k_{x1}})^2 + A(e^{\Gamma k_{x1}})^2$$

$$A = \frac{p_{x1}}{(e^{\Gamma k_{x1}})^2 - (e^{-\Gamma k_{x1}})^2}$$: So condition 1 and 2 are ok!

5 and 6:
x=k_{x3}:

$$p_3 = -\frac{C}{e^{-\Gamma k_{x3}}} e^{-\Gamma x} + \frac{C}{e^{\Gamma k_{x3}}} e^{\Gamma x}$$: So condition 6 is ok.

x=-k_{x3}:
Insert k_{x3} in the formula that's just found:

$$p_{x2} = -C(e^{\Gamma k_{x3}})^2 + C(e^{-\Gamma k_{x3}})^2$$

$$C = \frac{p_{x2}}{(e^{-\Gamma k_{x3}})^2 - (e^{\Gamma k_{x3}})^2}$$: So condition 5 and 6 are ok!

3 and 4:
x=-k_{x2}

$$p_2 = -\frac{B_{11}}{e^{\Gamma k_{x2}}} e^{-\Gamma x} + \frac{B_{22}}{e^{-\Gamma k_{x2}}} e^{\Gamma x} - \frac{1}{2} n(s\sigma)L$$

insert x=-k_{x2} in the formula just found:

$$p_{x1} = -B_{11} + B_{22} - \frac{1}{2} n(s\sigma)L$$

So:

$$B_{11} = -p_{x1} + B_{22} - \frac{1}{2} n(s\sigma)L$$

Insert x=k_{x2} in the formula found 5 lines back:

$$p_{x2} = -B_{11}(e^{-\Gamma k_{x2}})^2 + B_{22}(e^{\Gamma k_{x2}})^2 - \frac{1}{2} n(s\sigma)L$$

Insert the equation for B_{11} in the formula just found:

$$0 = -(-p_{x1} + B_{22} - \frac{1}{2} n(s\sigma)L)(e^{-\Gamma k_{x2}})^2 + B_{22}(e^{\Gamma k_{x2}})^2 - \frac{1}{2} n(s\sigma)L - p_{x2}$$

Rewritten:

$$0 = -B_{22}((e^{-\Gamma k_{x2}})^2 - (e^{\Gamma k_{x2}})^2) + (\frac{1}{2} n(s\sigma)L + p_{x1})(e^{-\Gamma k_{x2}})^2 - \frac{1}{2} n(s\sigma)L - p_{x2}$$

So B_{22}:

$$0 = -B_{22}((e^{-\Gamma k_{x2}})^2 - (e^{\Gamma k_{x2}})^2) + (\frac{1}{2} n(s\sigma)L + p_{x1})(e^{-\Gamma k_{x2}})^2 - \frac{1}{2} n(s\sigma)L - p_{x2}$$

$$B_{22} = \frac{\frac{1}{2} n(s\sigma)L((e^{-\Gamma k_{x2}})^2 - 1) + p_{x1}(e^{-\Gamma k_{x2}})^2 - p_{x2}}{(e^{-\Gamma k_{x2}})^2 - (e^{\Gamma k_{x2}})^2}$$

So B_{11}:

$$B_{11} = \frac{\frac{1}{2} n(s\sigma)L((e^{-\Gamma k_{x2}})^2 - 1) + p_{x1}(e^{-\Gamma k_{x2}})^2 - p_{x2}}{(e^{-\Gamma k_{x2}})^2 - (e^{\Gamma k_{x2}})^2} - p_{x1} - \frac{1}{2} n(s\sigma)L$$

Now 3 an 4 are ok!

7 with x=k_{x1} and -k_{x2}:

$$A\Gamma(e^{-\Gamma k_{x1}})^2 + A\Gamma(e^{\Gamma k_{x1}})^2 = B_{11}\Gamma + B_{22}\Gamma$$

8 with x=-k_{x3} and k_{x2}:

$$C\Gamma(e^{\Gamma k_{x3}})^2 + C\Gamma(e^{-\Gamma k_{x3}})^2 = B_{11}\Gamma(e^{-\Gamma k_{x2}})^2 + B_{22}\Gamma(e^{\Gamma k_{x2}})^2$$

A, B_{11} and B_{22} inserted in 7:

$$\frac{p_{x1}\Gamma((e^{-\Gamma k_{x1}})^2 + (e^{\Gamma k_{x1}})^2)}{(e^{\Gamma k_{x1}})^2 - (e^{-\Gamma k_{x1}})^2} = -p_{x1}\Gamma - \frac{1}{2} n(s\sigma)L\Gamma + \frac{\Gamma n(s\sigma)L((e^{-\Gamma k_{x2}})^2 - 1) + 2\Gamma p_{x1}(e^{-\Gamma k_{x2}})^2 - 2\Gamma p_{x2}}{(e^{-\Gamma k_{x2}})^2 - (e^{\Gamma k_{x2}})^2}$$

Rewritten:

$$p_{x1}\left(\frac{\Gamma((e^{-\Gamma k_{x1}})^2 + (e^{\Gamma k_{x1}})^2)}{(e^{\Gamma k_{x1}})^2 - (e^{-\Gamma k_{x1}})^2} + \Gamma - \frac{2\Gamma(e^{-\Gamma k_{x2}})^2}{(e^{-\Gamma k_{x2}})^2 - (e^{\Gamma k_{x2}})^2}\right) = -\frac{1}{2} n(s\sigma)L\Gamma + \frac{\Gamma n(s\sigma)L((e^{-\Gamma k_{x2}})^2 - 1)}{(e^{-\Gamma k_{x2}})^2 - (e^{\Gamma k_{x2}})^2} - \frac{2\Gamma p_{x2}}{(e^{-\Gamma k_{x2}})^2 - (e^{\Gamma k_{x2}})^2}$$

This can be written as p_{x1}=D1-p_{x2}D2-D3 with:

$$D1 = \frac{\frac{\Gamma n(s\sigma)L((e^{-\Gamma k_{x2}})^2 - 1)}{(e^{-\Gamma k_{x2}})^2 - (e^{\Gamma k_{x2}})^2}}{\left(\frac{\Gamma((e^{-\Gamma k_{x1}})^2 + (e^{\Gamma k_{x1}})^2)}{(e^{\Gamma k_{x1}})^2 - (e^{-\Gamma k_{x1}})^2} + \Gamma - \frac{2\Gamma(e^{-\Gamma k_{x2}})^2}{(e^{-\Gamma k_{x2}})^2 - (e^{\Gamma k_{x2}})^2}\right)}$$

$$D2=\frac{\frac{2\Gamma}{(e^{-\Gamma k_{x2}})^2-(e^{\Gamma k_{x2}})^2}}{\left(\frac{\Gamma((e^{-\Gamma k_{x1}})^2+(e^{\Gamma k_{x1}})^2)}{(e^{\Gamma k_{x1}})^2-(e^{-\Gamma k_{x1}})^2}+\Gamma-\frac{2\Gamma(e^{-\Gamma k_{x2}})^2}{(e^{-\Gamma k_{x2}})^2-(e^{\Gamma k_{x2}})^2}\right)}$$

$$D3=\frac{\frac{1}{2}n(s\sigma)L\Gamma}{\left(\frac{\Gamma((e^{-\Gamma k_{x1}})^2+(e^{\Gamma k_{x1}})^2)}{(e^{\Gamma k_{x1}})^2-(e^{-\Gamma k_{x1}})^2}+\Gamma-\frac{2\Gamma(e^{-\Gamma k_{x2}})^2}{(e^{-\Gamma k_{x2}})^2-(e^{\Gamma k_{x2}})^2}\right)}$$

C, B_{11} and B_{22} inserted in 8:

$$\frac{p_{x2}}{(e^{-\Gamma k_{x3}})^2-(e^{\Gamma k_{x3}})^2}\Gamma\left((e^{\Gamma k_{x3}})^2+(e^{-\Gamma k_{x3}})^2\right)=\left(\frac{\frac{1}{2}n(s\sigma)L((e^{-\Gamma k_{x1}})^2-1)+p_{x1}(e^{-\Gamma k_{x2}})^2-p_{x2}}{(e^{-\Gamma k_{x2}})^2-(e^{\Gamma k_{x2}})^2}-p_{x1}-\frac{1}{2}n(s\sigma)L\right)\Gamma(e^{-\Gamma k_{x2}})^2+\left(\frac{\frac{1}{2}n(s\sigma)L((e^{-\Gamma k_{x2}})^2-1)+p_{x1}(e^{-\Gamma k_{x2}})^2-p_{x2}}{(e^{-\Gamma k_{x2}})^2-(e^{\Gamma k_{x2}})^2}\right)\Gamma(e^{\Gamma k_{x2}})^2$$

Rewritten:

$$p_{x2}\left(\frac{\Gamma\left(e^{\Gamma k_{x3}})^2+(e^{-\Gamma k_{x3}})^2\right)}{(e^{-\Gamma k_{x3}})^2-(e^{\Gamma k_{x3}})^2}+\frac{\Gamma(e^{-\Gamma k_{x2}})^2+\Gamma(e^{\Gamma k_{x2}})^2}{(e^{-\Gamma k_{x2}})^2-(e^{\Gamma k_{x2}})^2}\right)=\frac{\frac{1}{2}n(s\sigma)L\Gamma((e^{-\Gamma k_{x2}})^2-1)((e^{-\Gamma k_{x2}})^2+(e^{\Gamma k_{x2}})^2)}{(e^{-\Gamma k_{x2}})^2-(e^{\Gamma k_{x2}})^2}-\frac{1}{2}n(s\sigma)L\Gamma(e^{-\Gamma k_{x2}})^2+p_{x1}\left(\frac{(e^{-\Gamma k_{x2}})^2(\Gamma(e^{-\Gamma k_{x2}})^2+\Gamma(e^{\Gamma k_{x2}})^2)}{(e^{-\Gamma k_{x2}})^2-(e^{\Gamma k_{x2}})^2}-\Gamma(e^{-\Gamma k_{x2}})^2\right)$$

This can be rewritten as: $p_{x2}=E1+E2+p_{x1}E3$ with:

$$E1=\frac{\frac{1}{2}n(s\sigma)L\Gamma((e^{-\Gamma k_{x2}})^2-1)((e^{-\Gamma k_{x2}})^2+(e^{\Gamma k_{x2}})^2)}{(e^{-\Gamma k_{x2}})^2-(e^{\Gamma k_{x2}})^2}$$
$$\left(\frac{\Gamma\left((e^{\Gamma k_{x3}})^2+(e^{-\Gamma k_{x3}})^2\right)}{(e^{-\Gamma k_{x3}})^2-(e^{\Gamma k_{x3}})^2}+\frac{\Gamma(e^{-\Gamma k_{x2}})^2+\Gamma(e^{\Gamma k_{x2}})^2}{(e^{-\Gamma k_{x2}})^2-(e^{\Gamma k_{x2}})^2}\right)$$

$$E2=\frac{-\frac{1}{2}n(s\sigma)L\Gamma(e^{-\Gamma k_{x2}})^2}{\left(\frac{\Gamma\left((e^{\Gamma k_{x3}})^2+(e^{-\Gamma k_{x3}})^2\right)}{(e^{-\Gamma k_{x3}})^2-(e^{\Gamma k_{x3}})^2}+\frac{\Gamma(e^{-\Gamma k_{x2}})^2+\Gamma(e^{\Gamma k_{x2}})^2}{(e^{-\Gamma k_{x2}})^2-(e^{\Gamma k_{x2}})^2}\right)}$$

$$E3=\frac{\left(\frac{(e^{-\Gamma k_{x2}})^2(\Gamma(e^{-\Gamma k_{x2}})^2+\Gamma(e^{\Gamma k_{x2}})^2)}{(e^{-\Gamma k_{x2}})^2-(e^{\Gamma k_{x2}})^2}-\Gamma(e^{-\Gamma k_{x2}})^2\right)}{\left(\frac{\Gamma\left((e^{\Gamma k_{x3}})^2+(e^{-\Gamma k_{x3}})^2\right)}{(e^{-\Gamma k_{x3}})^2-(e^{\Gamma k_{x3}})^2}+\frac{\Gamma(e^{-\Gamma k_{x2}})^2+\Gamma(e^{\Gamma k_{x2}})^2}{(e^{-\Gamma k_{x2}})^2-(e^{\Gamma k_{x2}})^2}\right)}$$

Now it is possible to rewrite the equations for p_{x1} and p_{x2}:
p_{x2}=(E1+E2+D1E3-D3E3)/(1+D2E2)
p_{x1}=D1-((E1+E2+D1E3-D3E3)/(1+D2E2))D2-D3

So all the 8 unknowns (A1, A2, B1, B2, C1, C2, p_{x1} and p_{x2}) are known, which means that the pressure in the 3 tubes can be calculated.

Appendix E: Results comparison

In this appendix the results of the comparison between the model and the experiments will be given for the sound pressure level in the tube and the far field pressure.

Data experiments:

X_data=[0.18 0.16 0.14 0.12 0.1 0.08 0.06 0.04];
Data_meas_1000=[90.2 101.5 104.95 105.75 106.4 105.25 103.35 96.27];
acceleration=0.28
Data_meas_500=[96.9 108.86 113 115.3 117.56 118.8 119.93 120.24];
acceleration =0.18
Data_meas_250=[87.4 98.34 102.77 105.065 107.6 108.92 110.693 111.84];
acceleration =0.137
Data_meas_750=[85.73 94.727 101.15 100.5 101.74 102.7 103.33 103.1];
acceleration =0.177 (between 0.165-0.19)
Data_meas_1250=[101.3 112.32 115.5 116 115.255 111.327 101.15 106];
acceleration =0.36 (between 0.32-0.4)
Data_meas_1500=[94.79 106.31 108.845 108.51 105.89 94.975 100.276 107.51];
acceleration =0.45 (between 0.4-0.5)
Data_meas_1750=[97.354 108.177 110.3 108.15 100.88 98.96 108.08 110.025];
acceleration =0.73 (between 0.68-0.76)
Data_meas_2000=[89.7 100.8 102.24 98.31 80.53 98.41 102.22 100.35];
acceleration =0.35 (between 0.3-0.40)
Data_meas_2250=[96.97 107.03 107.15 96.95 101.9 107.4 106.04 90];
acceleration =0.25 (between 0.14-0.35)
Data_meas_2500=[81.6 91.377 89.7 76.65 90.4 91.25 83.242 87.4];
acceleration =(0.12 (estimation))

Sound pressure level (re 5e-5 Pa):

In each graph there are 4 frequencies. The figure at the left-bottom is the frequency/1.15. The figure at the left-top is (frequency/1.15)-40, the figure at the right top is (frequency/1.15)-10 and the figure at the right bottom is the (frequency/1.15)+30.

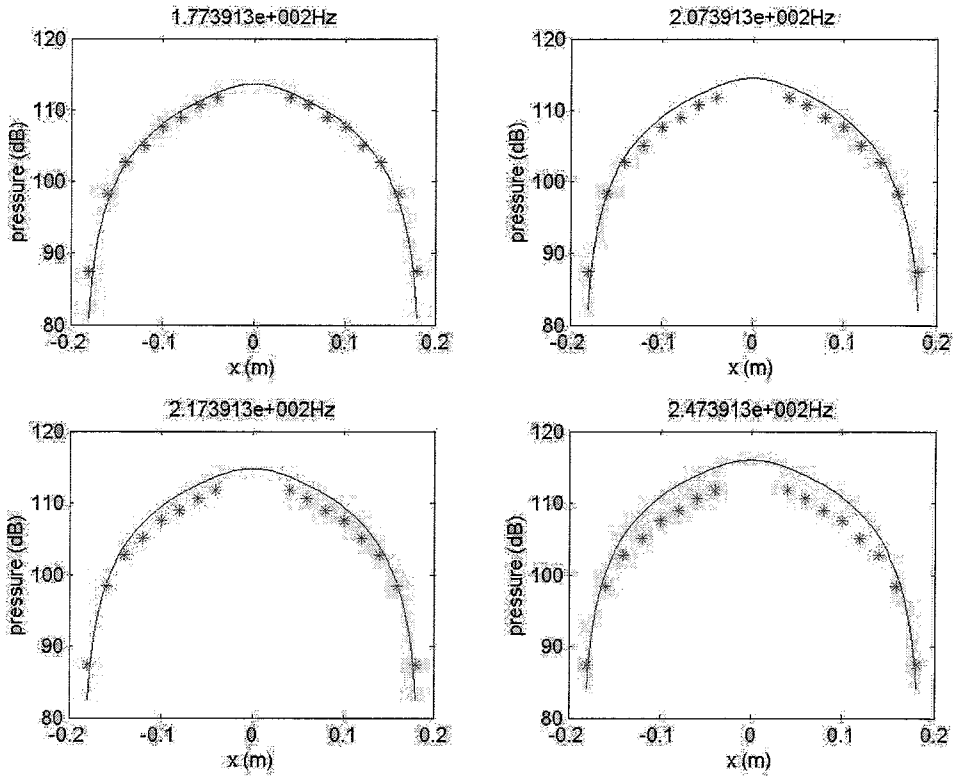

Measurement at 250 Hz

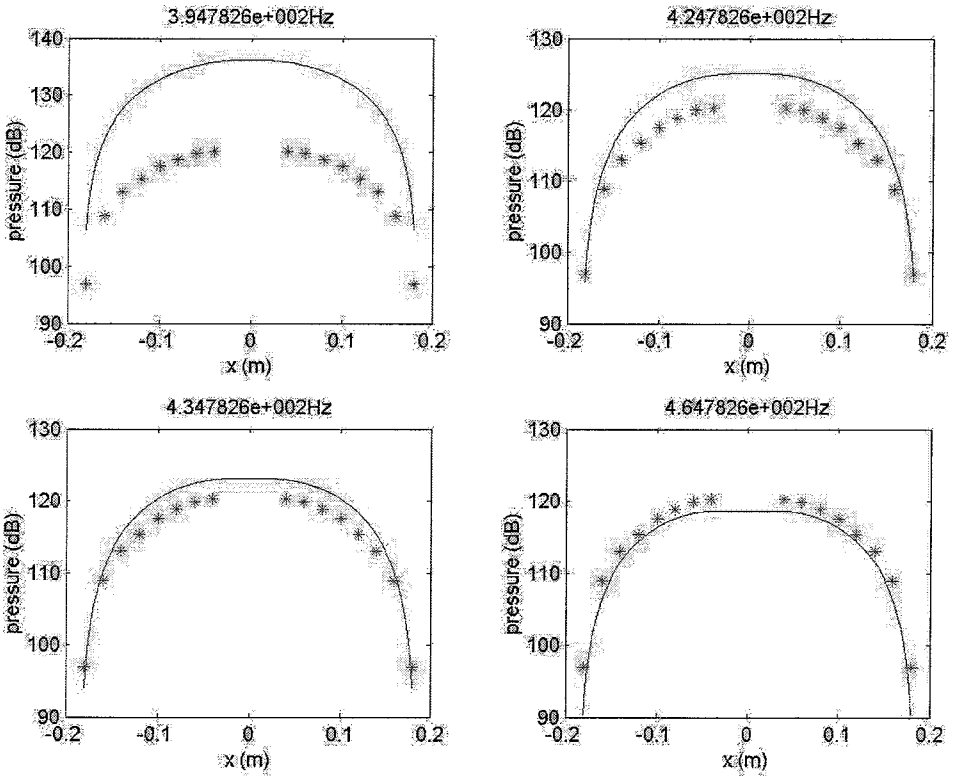

Measurement at 500Hz

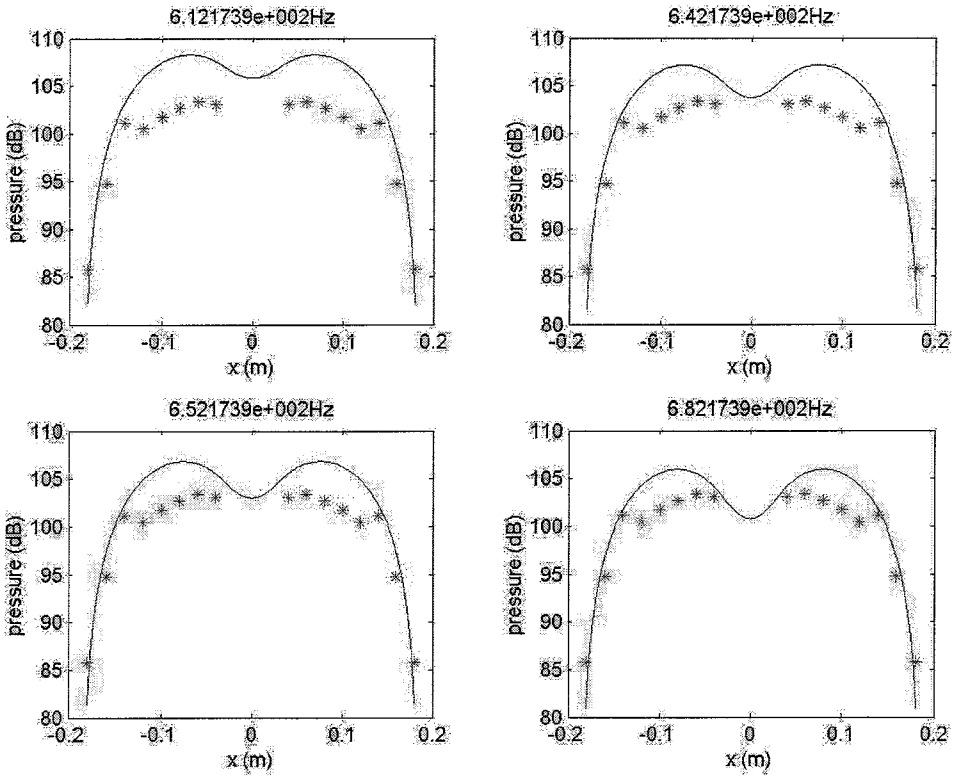

Measurement at 750 Hz

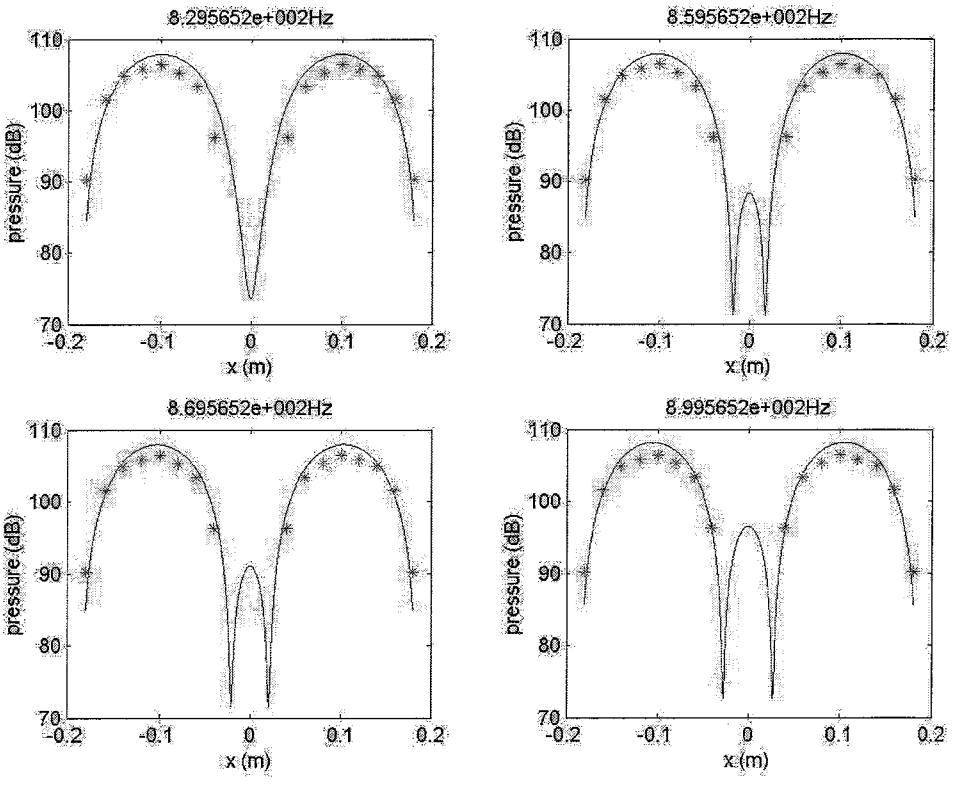

Measurement at 1000 Hz

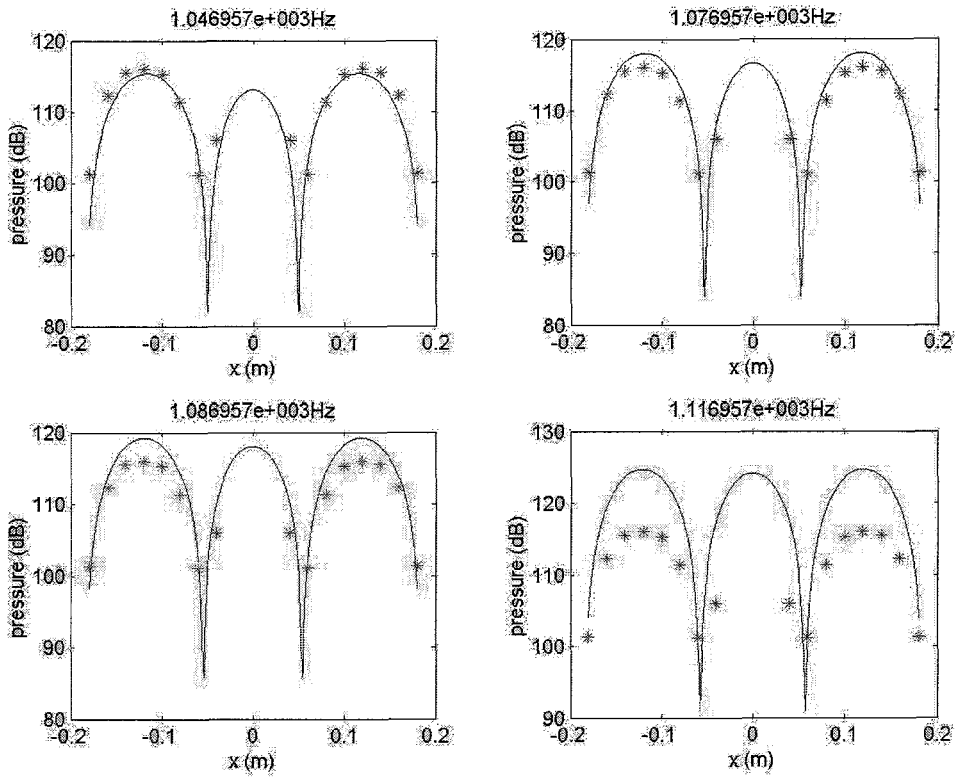

Measurement at 1250 Hz

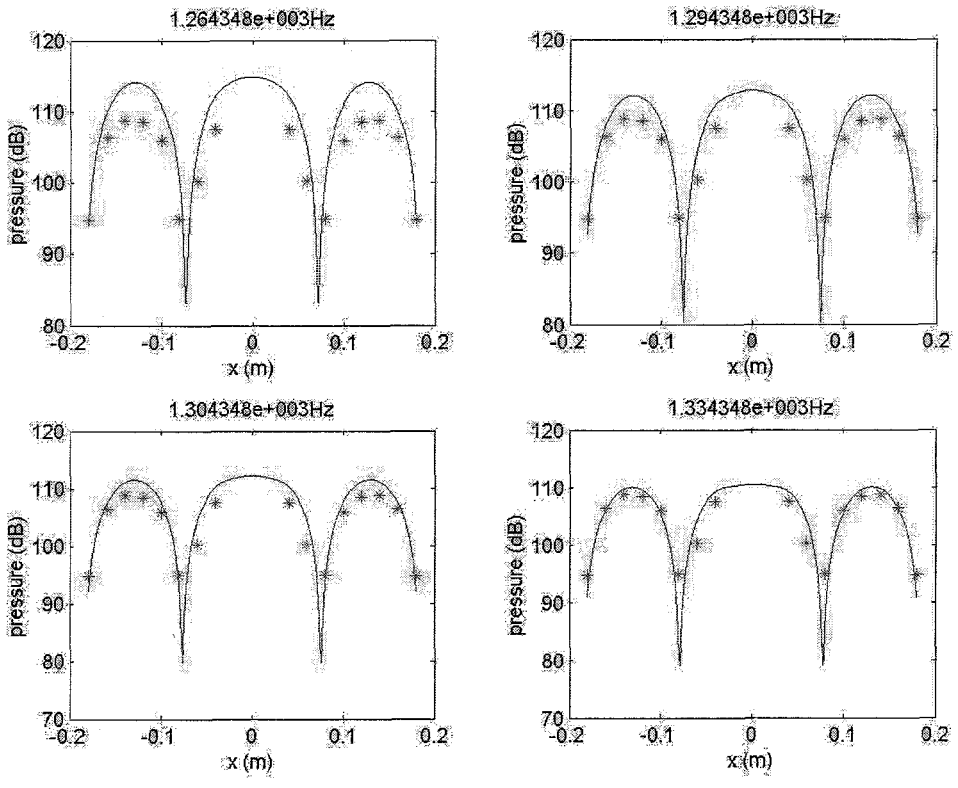

Measurement at 1500 Hz

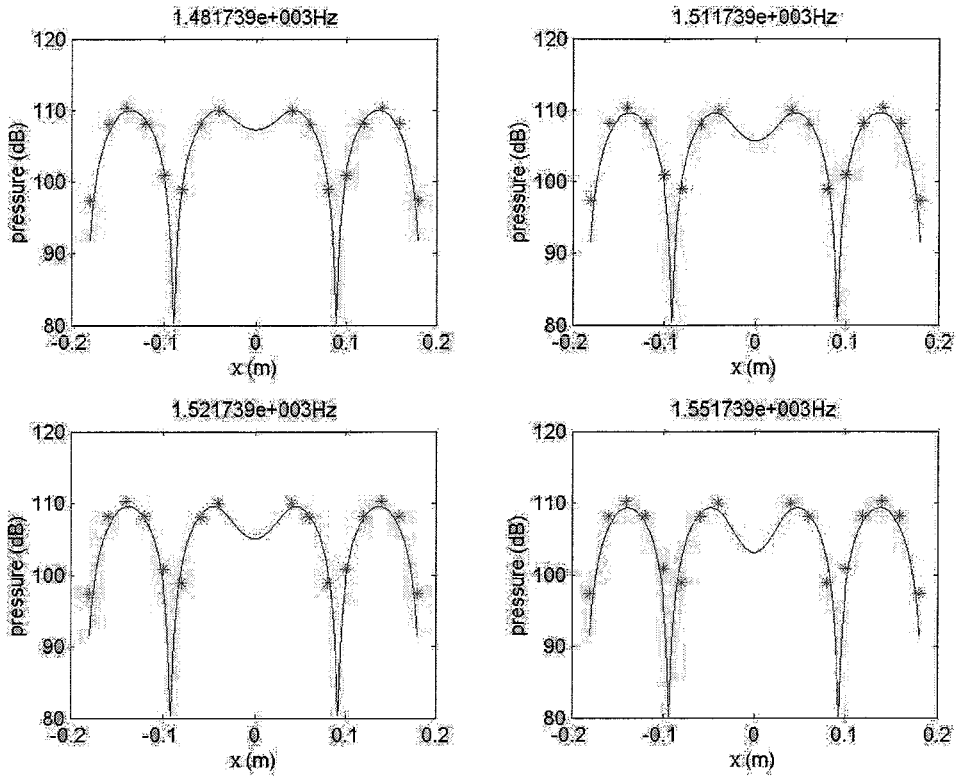

Measurement at 1750 Hz

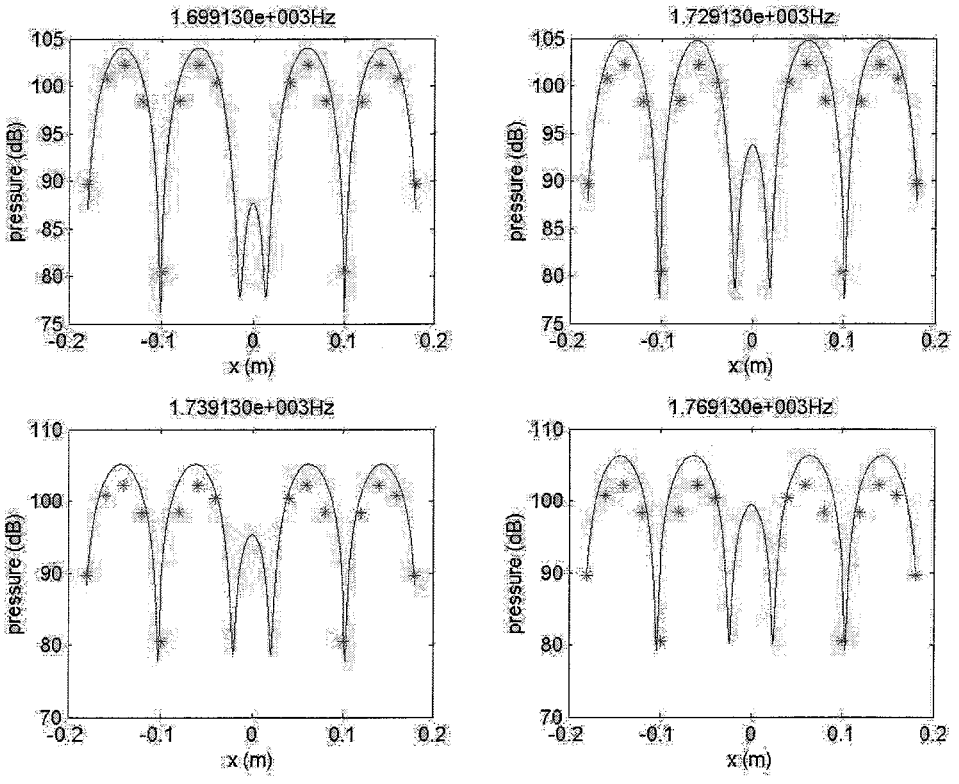

Measurement at 2000 Hz

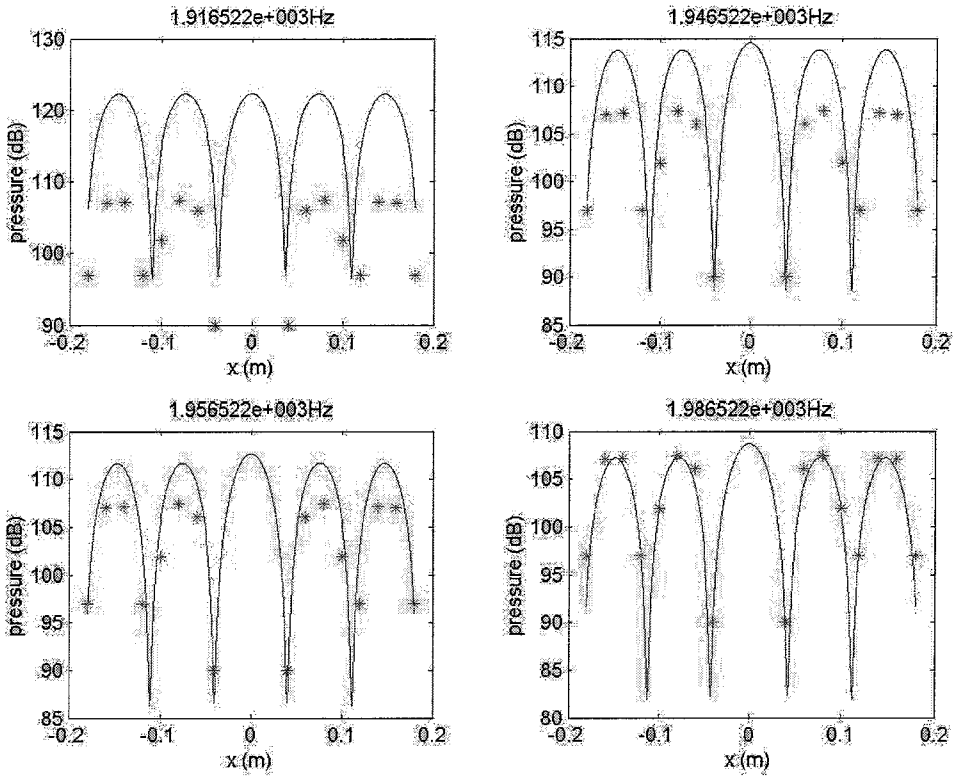

Measurement at 2250 Hz

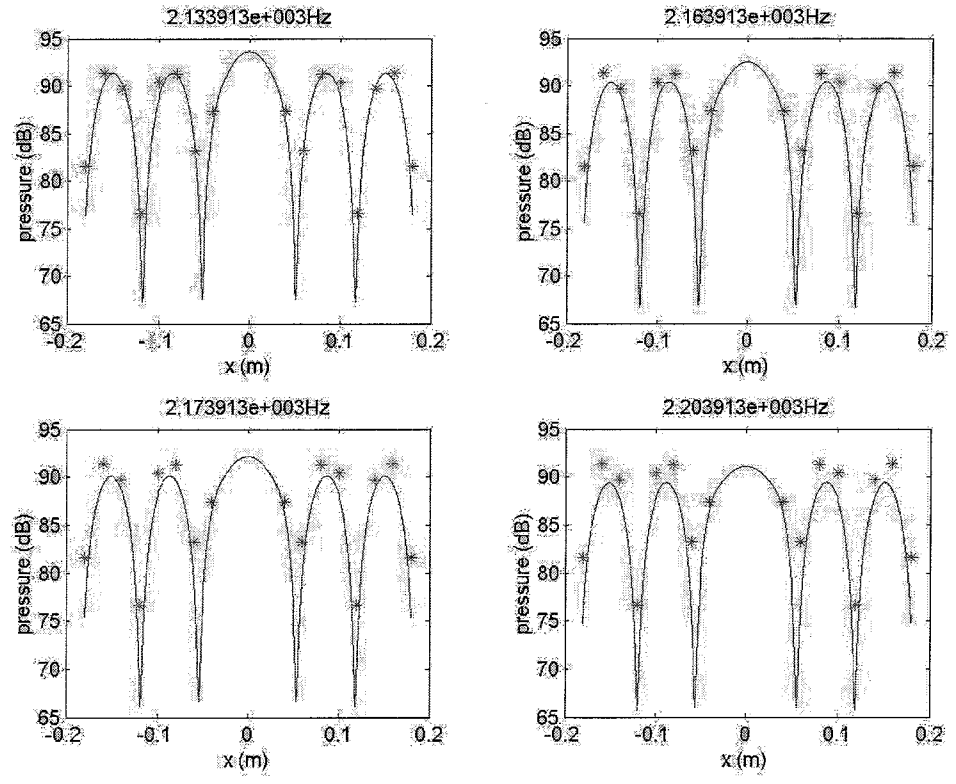

Measurement at 2500 Hz

Appendix F: B function

After some research it appeared that the value of the function B (function 19), as given in [1], does not convert to –1 but to –0.74 for high values of the shear wave number. It is expected to convert to –1, because:

- It is stated in [1] and appendix D that B should go to –1 for high shear wave numbers.
- B is defined as: $B(s) = \frac{1}{A^{cd}} \int_{A^{cd}} A(s, x^{cd}) dA^{cd}$ (19)

  It is known from earlier calculations that A is –1 (absolute value is 1) over almost the whole area, because the piston approximation is based upon this. So over the whole area there is a value –1, so if one than integrates A over the whole area and divides again over the whole area one gets a value of –1 for B.
- By numeritical integration of A over the whole area and than dividing by the area also the result of –1 for high shear wave numbers is achieved.
- The value of B for the expression for a tube with a circular cross-section [1] also goes to –1 for high shear wave numbers.

In figure F.1 the following 4 B functions will be shown; The original one as used in [1], the original one divided by a factor to bring it to –1, the B formula for a round tube and the B formula derived by numeritical integration of A.

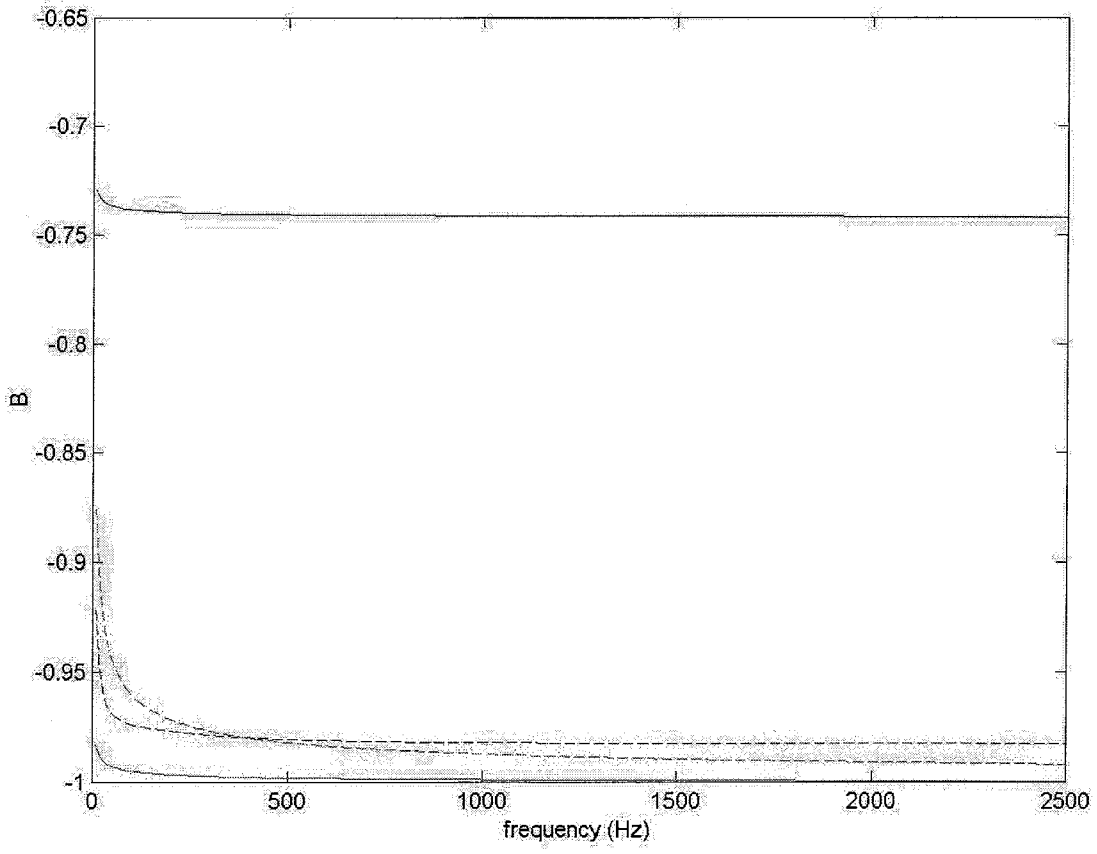

Figure F.1: Different B formula's (dark solid=original B form [1], dark dashed=B determined with a numeritical integration, light solid=original B from [1] divided by a factor and light dashed=B from a tube with a round cross-section [1])

Because there is a strange difference between the B formula of [1] and what could be expected it is chosen to perform a calculation of the transfer function of the tube of 360 mm with the 4 different B functions described in figure F.1. Figure F.2 shows the result of this calculation.

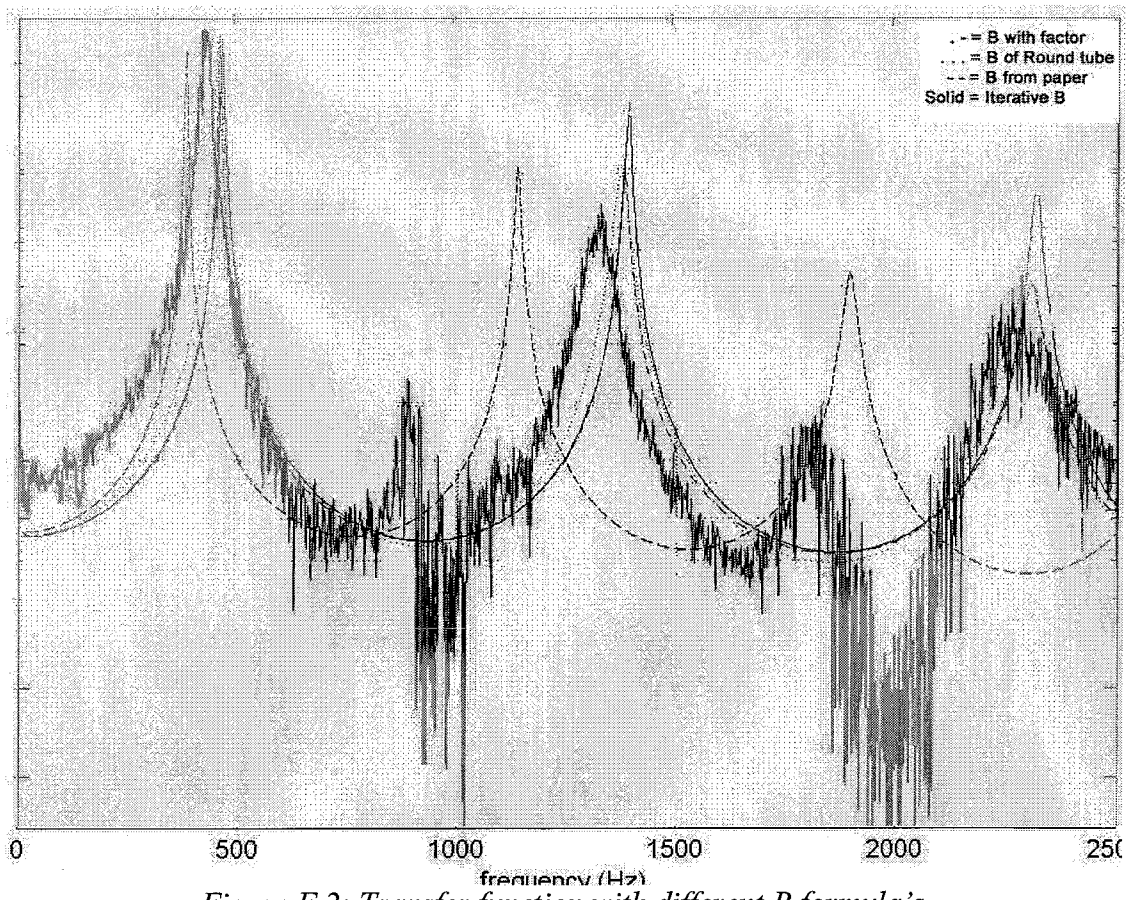

Figure F.2: Transfer function with different B formula's

What can be concluded from figure F.2 is that there is a better match between the results from the model and the experiments with the 3 "new" B formulas. However there is now an over prediction of the eigenfrequency instead of an under prediction. This over prediction of about 2% can be explained by the fact that the measurement is performed with a tube without a good baffled end, so there is more leakage out of the system than there would be with a good baffled end system. This can be a reason why the frequencies do not completely match. What also can be a reason is that the impedance of the model is maybe a bit to low, because the impedance "virtually" lengthens the tube, so if the impedance is larger the "virtual" tube gets longer and thus the eigenfrequency decreases.
What also can be concluded from the figure is that the overall transfer-function looks the same for the "old" B from [1] and the new "B's", only the frequency is different. This is at least true for the case of the B from the round tube and the B with the factor. Only the transfer function with the B determined on an iterative way is a bit different. This can be because the iteration is not good enough at the edges of the opening of the tube.

Appendix G: Validation boundary condition

In this appendix the p=0 boundary condition in model A will be validated using the end-impedance used in model B.

There the "opening" of the layers has a maximum of 40mm x 5 mm (20mm x 20mm x 5mm patch translated in a tube with 2 openings of 40mm x 5mm).
The reflection factor is –0.8 at 2000 Hz and –0.5 at 4000 Hz for this opening. This is a large factor, but on the other hand it is the maximum factor for a tyre tread as defined in model A. The smaller the gap the more the factor will go to –1. With this in mind it is possible to conclude that for the largest tread block with the maximum gap size it is important to have a high amplitude, because than the pressure at the center is not that much affected by the leakage at the sides. However for smaller tread blocks and smaller gaps the reflection factor nears –1, so than the boundary condition of p=0 is valid. The conclusion can be that also for some smaller amplitude the calculation will be valid.